Geology Faculty Publications   Geology

10-12-2021

Metamorphism of the Sierra de Maz and implications for the tectonic evolution of the MARA terrane

Andrew Tholt
Western Washington University, tholta@wwu.edu

Sean R. Mulcahy
Western Washington University, sean.mulcahy@wwu.edu

William C. McClelland

Sarah M. Roeske

Vinícius T. Meira

See next page for additional authors

Recommended Citation

Authors

Andrew Tholt, Sean R. Mulcahy, William C. McClelland, Sarah M. Roeske, Vinícius T. Meira, Patricia Webber, Emily Houlihan, Matthew A. Coble, and Jeffrey D. Vervoort

Metamorphism of the Sierra de Maz and implications for the tectonic evolution of the MARA terrane

Andrew Tholt[1], Sean R. Mulcahy[1], William C. McClelland[2], Sarah M. Roeske[3], Vinícius T. Meira[4], Patricia Webber[2], Emily Houlihan[3], Matthew A. Coble[4], and Jeffrey D. Vervoort[5]

[1]Geology Department, Western Washington University, Bellingham, Washington 98225, USA
[2]Department of Geoscience, University of Iowa, Iowa City, Iowa 52242, USA
[3]Department of Earth and Planetary Sciences, University of California, Davis 95616, California, USA
[4]Department of Geology and Natural Resources, Institute of Geosciences, University of Campinas (UNICAMP), Campinas 13083-855, Brazil
[5]Department of Geological Sciences, Stanford University, Stanford, California 94305, USA
[6]School of the Environment, Washington State University, Pullman, Washington 99164, USA

ABSTRACT

The Mesoproterozoic MARA terrane of western South America is a composite igneous-metamorphic complex that is important for Paleozoic paleogeographic reconstructions and the relative positions of Laurentia and Gondwana. The magmatic and detrital records of the MARA terrane are consistent with a Laurentian origin; however, the metamorphic and deformation records lack sufficient detail to constrain the correlation of units within the MARA terrane and the timing and mechanisms of accretion to the Gondwana margin.

Combined regional mapping, metamorphic petrology, and garnet and monazite geochronology from the Sierra de Maz of northwest Argentina suggest that the region preserves four distinct litho-tectonic units of varying age and metamorphic conditions that are separated by middle- to lower-crustal ductile shear zones. The Zaino and Maz Complexes preserve Barrovian metamorphism and ages that are distinct from other units within the region. The Zaino and Maz Complexes both record metamorphism ca. 430–410 Ma and show no evidence of the regional Famatinian orogeny (ca. 490–455 Ma). In addition, the Maz Complex records an earlier granulite facies event at ca. 1.2 Ga. The Taco and Ramaditas Complexes, in contrast, experienced medium- and low-pressure upper amphibolite to granulite facies metamorphism, respectively, between ca. 470–460 Ma and were later deformed at ca. 440–420 Ma.

The Maz shear zone that bounds the Zaino and Maz Complexes records sinistral oblique to sinistral deformation between ca. 430–410 Ma. The data suggest that at least some units in the MARA terrane were accreted by translation, and the Gondwana margin of northwest Argentina transitioned from a dominantly convergent margin to a highly oblique margin in the Silurian.

■ INTRODUCTION

The western margin of South America preserves a little understood and complex orogenic belt that is critical to Paleozoic paleogeographic reconstructions

Sean R. Mulcahy https://orcid.org/0000-0002-8506-178X

and the relative positions of Laurentia and Gondwana. Basement terranes within the Western Sierras Pampeanas of northwest Argentina, located between the allochthonous Precordillera terrane to the west and the Cambrian-Ordovician continental Famatina arc to the east (Fig. 1), record a prolonged history of magmatism (e.g., Vujovich and Kay, 1998; Rapela et al., 2010, 2018; Varela et al., 2011; Ramos, 2018; Ramacciotti et al., 2019a), metamorphism (e.g., Casquet et al., 2001; Otamendi et al., 2008; Mulcahy et al., 2014), and deformation (e.g., Ramos et al., 1998; Mulcahy et al., 2007, 2011; Meira et al., 2012; Garber et al., 2014). Rapela et al. (2010) distinguished two different domains within the Western Sierras Pampeanas (Fig. 1): a Mesoproterozoic (1.2–1.03 Ga) oceanic mafic-ultramafic domain largely exposed along the western margin of the Sierra de Pie de Palo and a Paleoproterozoic continental domain that was reworked in the Mesoproterozoic (1.3–1.05 Ga), has a Neoproterozoic sedimentary cover, and is exposed in the central and eastern margin of the Sierra de Pie de Palo and the Sierras de Maz, Umango, and Espinal. The Paleoproterozoic continental domain has ages and isotope compositions similar to those of the Arequipa massif in Peru and the Rio Apa in Brazil. On this basis, portions of the Sierras de Maz, Umango, Espinal, Arequipa massif, and Rio Apa have been inferred as having a similar origin and are referred to as the MARA terrane (e.g., Casquet et al., 2012). The magmatic and detrital records of basement exposures within the MARA block suggest the terrane rifted from Laurentia around 570 Ma and subsequently collided and was partially subducted beneath the Rio de la Plata craton at ca. 530 Ma (e.g., Casquet et al., 2012; Rapela et al., 2016). Evidence for a ca. 530 Ma collision is indirectly inferred from cessation of arc volcanism within the Rio de la Plata craton (Rapela et al., 2016), but direct evidence for this event is largely absent within the MARA block itself.

Much of the evidence for the geologic history of the MARA block within the Western Sierras Pampeanas comes from exposures within the Sierra de Maz (Figs. 1–2), where lithologic units separated and deformed by middle- to lower-crustal high-strain zones variably record two metamorphic events at ca. 1.2 Ga and between 460 Ma and 430 Ma (e.g., Lucassen and Becchio, 2003; Casquet et al., 2006). Despite previous work, the metamorphic age and conditions of individual litho-tectonic units and the timing and kinematics of deformation on unit-bounding shear zones are not well constrained.
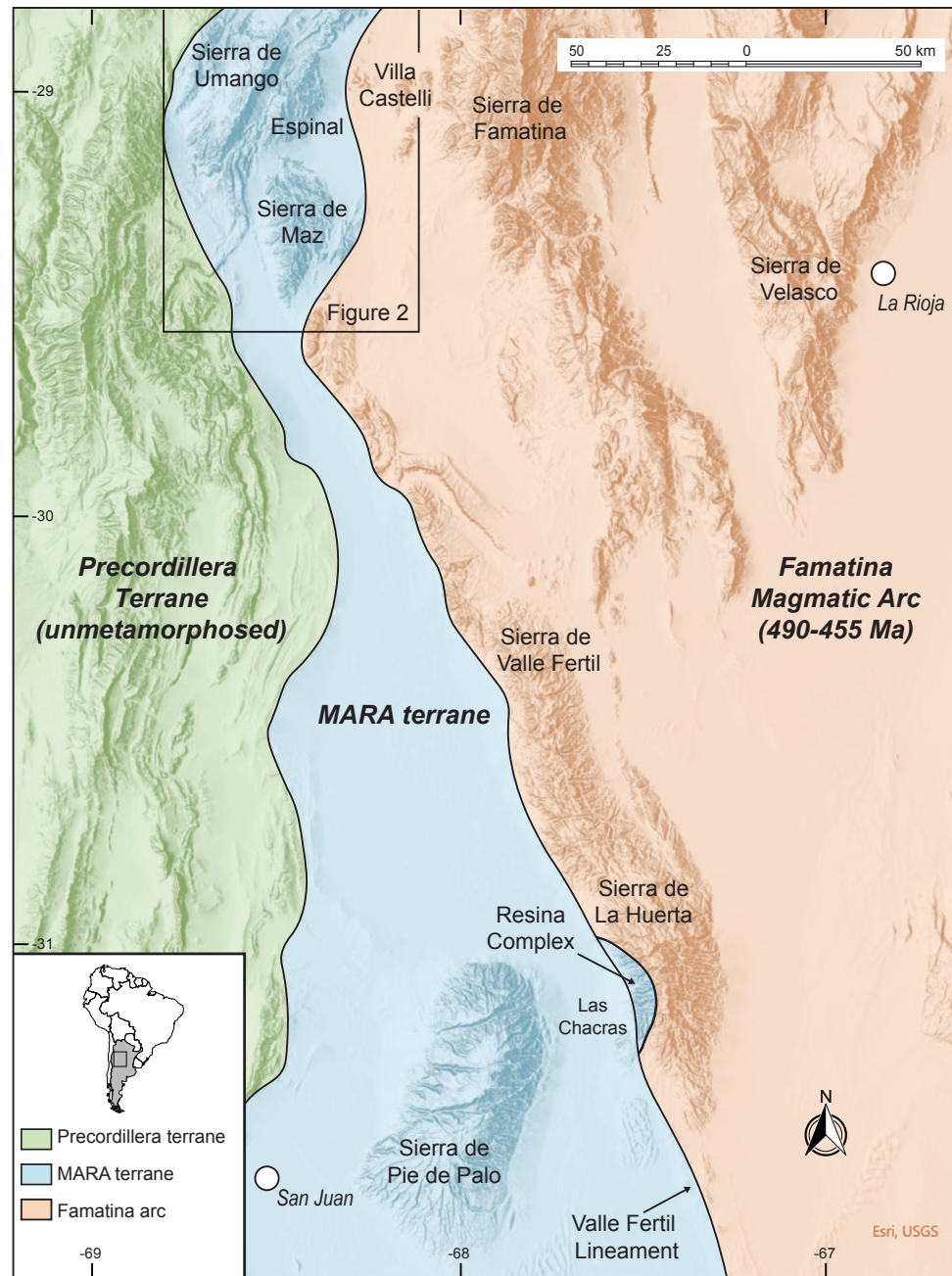
Figure 1. Tectonic map of the Western Sierras Pampeanas of northwest Argentina. The map depicts the generally accepted grouping of all metamorphic rocks between the Precordillera terrane and Famatina arc as the MARA terrane. Inset of South America in the figure legend shows the approximate location of the map area. Geographic regions discussed in the text are shown for reference, and the inset shows the location of Figure 2.

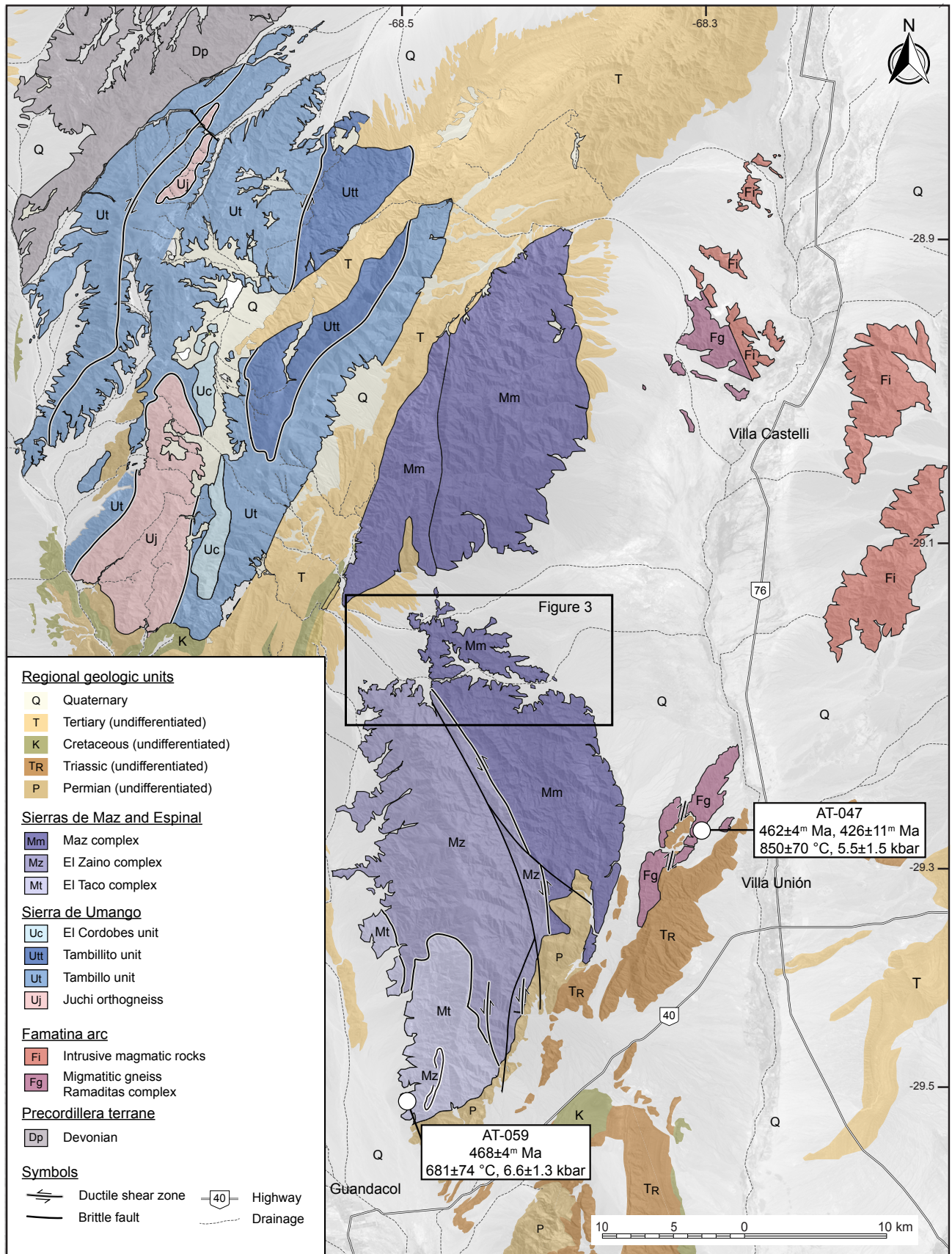Figure 2. This geologic map of the Sierras de Umango, Espinal, and Maz was adapted from published maps (e.g., Porcher et al., 2004; Casquet et al., 2006; Varela et al., 2011; Meira et al., 2012) and the mapping conducted in this work. Geochronology sample locations in the Taco and Ramaditas Complexes are shown. A detailed geologic map with additional sample locations is outlined in the inset box and shown in Figure 3.

We combine regional mapping, metamorphic petrology, and garnet and monazite geochronology to constrain the conditions and timing of metamorphism and deformation within each unit of the Sierra de Maz. The data suggest that the region preserves four distinct litho-tectonic units of varying ages and metamorphic conditions that are separated by distinct middle- to lower-crustal ductile shear zones. At least two prominent units within the Sierra de Maz lack metamorphic ages associated with the Famatinian orogeny (490–455 Ma) and instead record a Silurian–Devonian metamorphic event (430–410 Ma) that is likely related to a transition from highly oblique convergence to translation along the Famatina margin.

■ GEOLOGY OF THE SIERRA DE MAZ

The Sierra de Maz is located between the allochthonous Cambrian-Ordovician Precordillera terrane and the Ordovician Famatina continental magmatic arc of the Gondwana margin (Figs. 1–2). The region was first described by Kilmurray and Dalla Salda (1971) as three sub-parallel metamorphic domains trending NNW-SSE that are separated by first-order faults and shear zones. From west to east, previous workers have divided the domain into distinct units, namely the Taco Complex, the Zaino Complex, and the Maz Complex; however, these units have been variably mapped and correlated within the Sierra de Maz. These units are unconformably overlain by horizontal, unmetamorphosed Triassic sedimentary rocks (Fig. 2), indicating that Cretaceous and younger Andean deformation has had little effect on the orientation of structures within the metamorphic units of the Sierra de Maz.

Litho-Tectonic Units

We recognize four distinct litho-tectonic units—modified from previous workers (e.g., Kilmurray and Dalla Salda, 1971; Porcher et al., 2004; Casquet et al., 2008b) and based on protolith, mineral assemblage, and metamorphic grade—that are separated from one another by ductile shear zones and/or faults. From west to east and from low- to high-structural levels the units are the Taco Complex, the Zaino Complex, the Maz Complex, and the Ramaditas Complex (Figs. 2–3).

The Taco Complex is exposed in the southwestern portion of the Sierra de Maz and is separated from the structurally higher Zaino Complex by an unstudied and unnamed low-angle structure (Fig. 2) that was mapped on the basis of satellite imagery and previously published maps (Varela et al., 2011). In this region, the Taco Complex contains variably deformed Sil-Grt-Bt ± Ms ± Kfs schist and gneiss (Fig. 4A) (mineral abbreviations after Whitney and Evans, 2010), quartzite, Bt-Plg-Amp ± Grt amphibolite, felsic to intermediate orthogneiss, and thick (≤10 m) layers of marble. Lucassen and Becchio (2003) obtained titanite U-Pb ages of 533 ± 4 Ma and 443 ± 3 Ma from calcsilicate in this region of the Taco Complex and interpreted the range of ages to reflect long-standing, high-temperature conditions in the middle crust of the Famatina arc.

The Zaino Complex is exposed in the northwest and central regions of the Sierra de Maz and is separated from the Maz Complex to the east by the Maz shear zone (Figs. 2–3). The Zaino Complex contains pelitic and calc-silicate schist, marble, and lesser amphibolite. In the north (Fig. 3), Pl-Qz-Bt-Ms pelitic schist varies from the chlorite zone in the west (Fig. 4B) and progresses through the garnet zone (Fig. 4C) and into the staurolite zone to the east, which is adjacent to the Maz shear zone. The dominantly east-dipping foliation is deformed by shallowly N-plunging folds with steep NW-SE–striking axial planes (Fig. 3B). Casquet et al. (2008b) noted that the lithology of the Zaino Complex is similar to that of the Difunta Correa metasedimentary sequence of Sierra de Pie de Palo (Fig. 1), and Colombo et al. (2009) suggested the two units were likely equivalent, but this interpretation remains speculative due to the absence of protolith ages and few metamorphic ages from the Zaino Complex (as defined in this study).

The Maz Complex extends east from the Maz shear zone to the eastern boundary of the Sierra de Maz range front (Fig. 2). We have subdivided the Maz Complex into four parallel domains based on variations in the dominant protolith (Fig. 3). Immediately east of the Maz shear zone, domain Mm1 contains amphibolite, orthogneiss, and less commonly pelitic schist or gneiss. The pelitic schist and gneiss within Mm1 contain the assemblage Pl-St-Grt-Qz-Ms (Fig. 4D). Colombo et al. (2009) dated an 846 ± 6 Ma orthogneiss that they interpreted as the original protolith age within what we consider to be Mm1 of the Maz Complex. The next sequence to the east, Mm2, contains paragneiss, amphibolite, and interleaved orthogneiss. Paragneiss within Mm2 contains the assemblage Pl-St-Grt-Qz-Ms ± Ky, commonly with retrograde chlorite. The third domain, Mm3, contains massif-type anorthosite that was recognized and dated at 1070 ± 41 Ma by Casquet et al. (2005). Mm4, which lies along the eastern margin of the Maz Complex, contains intermediate to mafic orthogneiss, mafic granulite, Kfs-bearing augen gneiss, and Pl-Ms-Bt-Grt-Sil-Kfs ± St gneiss and migmatite (Fig. 4E). Casquet et al. (2008a) documented a Cambrian (ca. 570 Ma) syenite-carbonatite complex along the eastern margin of the range that we include with this unit. Foliation throughout the Maz Complex generally dips steeply to the east and is folded by northwest-southeast–plunging folds. Mineral lineations systematically become shallower from E to W across the Maz Complex approaching the Maz shear zone (Fig. 3). Lucassen and Becchio (2003) obtained titanite U-Pb ages of 1216 ± 63 Ma, 436 ± 22 Ma, and 428 ± 6 Ma from calcsilicate samples within the Maz Complex and did not assign the ages to a particular tectonic event. Similarly, Casquet et al. (2005, 2006) used zircon U-Pb geochronology to recognize two different metamorphic events within the Maz Complex: a granulite facies metamorphic event at 1208 ± 28 Ma and a younger event at 431 ± 40 Ma. In contrast, Porcher et al. (2004) reported two-point garnet Sm-Nd ages of 1030 ± 3 Ma and 463 ± 16 Ma. Estimates of metamorphic conditions within the Maz Complex range from 6.5 kbar to 7.8 kbar and 630–775 þC (Porcher et al., 2004; Casquet et al., 2006; Colombo et al., 2009; Lucassen et al., 2010).
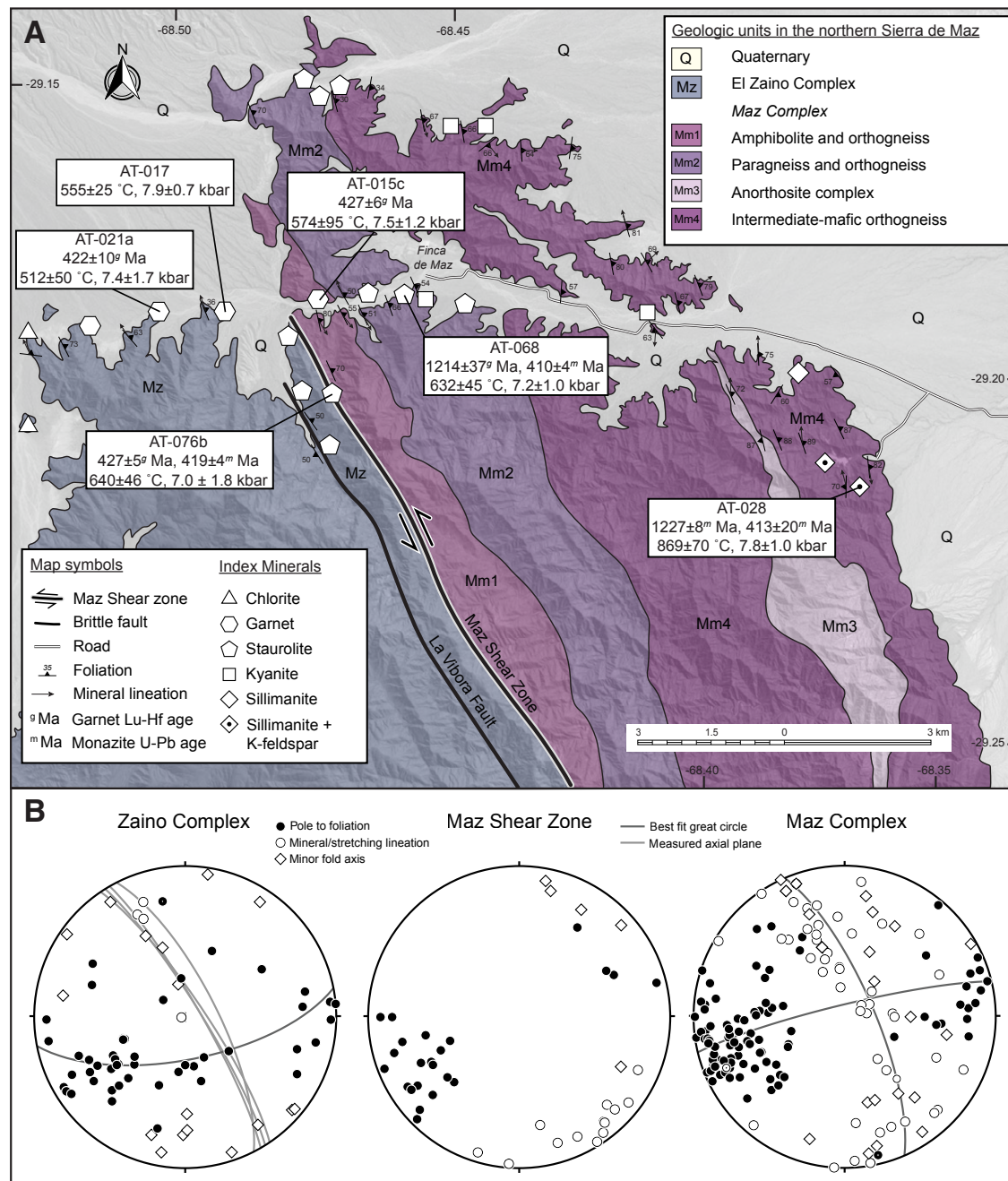
Figure 3. Detailed geologic map shows the northern Sierra de Maz. Locations of pressure-temperature estimates and garnet and monazite geochronology samples are shown. The mapped distribution of the anorthosite complex (Mm3) is taken from Casquet et al. (2006).

Figure 4. Outcrop photographs show units and assemblages from the Sierra de Maz and Sierra de Ramaditas. (A) Mylonitic Kfs-Sil-Grt-Bt schist (AT-059) of the Taco Complex; (B) chlorite zone schist of the Zaino Complex; (C) garnet zone schist (AT-021) of the Zaino Complex (small porphyroblasts are garnet); (D) staurolite zone schist of the Maz Complex and within the Maz shear zone that displays sinistral asymmetric tails on elongate staurolite; (E) sillimanite-K-feldspar gneiss (AT-028) of the Maz Complex; and (F) cordierite-bearing leucosome in migmatite of the Ramaditas Complex.

We define the Ramaditas Complex as the rocks exposed within the Sierras de Ramaditas, which is east of the Sierra de Maz range (Fig. 2). Previous authors have correlated this unit with either the Taco Complex (Kilmurray and Dalla Salda, 1971; Porcher et al., 2004) or with units farther north in Villa Castelli (Fig. 1) and/or the eastern portion of Sierra de Espinal (Fig. 2) (Casquet et al., 2006, 2008b; Colombo et al., 2009). Within the Sierras de Ramaditas, the unit consists of pelitic Kfs-Grt-Sil-Bt migmatite, intermediate-felsic orthogneiss, lesser amphibolite, and Grt-Scp-Cpx calc-silicates. Cordierite locally occurs as subhedral to anhedral grains with biotite and garnet in migmatitic melanosomes and as large euhedral pseudo-hexagonal grains in migmatitic leucosomes (Fig. 4F). The unit is isoclinally folded, and the dominant foliation dips to the east following the general trend of units within the Sierra de Maz. Weakly deformed to undeformed granitic dikes crosscut the dominant NNW-SSE foliation. In the northern extent of the Sierras de Ramaditas, Casquet et al. (2008b) reported a zircon U-Pb age of 442 ± 3 Ma from a calc-silicate gneiss that they interpreted as the metamorphic age of the unit. In contrast, Porcher et al. (2004) reported a two-point Sm-Nd garnet age of 301 ± 16 Ma from a metapelitic gneiss that they interpreted as peak

metamorphic age but also noted that the age could reflect cooling following peak conditions.

Previous workers recognized the existence of ductile shear zones and brittle faults throughout the Sierra de Maz (e.g., Kilmurray and Dalla Salda, 1971; Porcher et al., 2004; Casquet et al., 2005). In addition to the La Vibora brittle fault that occurs in the west-central portion of the Sierra de Maz (Fig. 3), we recognize two prominent ductile shear zones that are described below.

The Maz shear zone is a ductile shear zone that separates the Zaino Complex in the west from the Maz Complex in the east (Figs. 2–3). The shear zone is defined by a ~1-km-wide zone of steeply east-dipping mylonite and ultramylonite (Fig. 5A) with moderate to shallowly southeast-plunging mineral lineations (Fig. 3) that intensify as one approaches the shear zone, overprinting an older fabric within the Maz Complex (Fig. 5B). Asymmetric tails on garnet and staurolite porphyroblasts (Figs. 4D and 6A) and mica fish indicate a sinistral sense of shear. While the Maz shear zone is a prominent mylonite-ultramylonite zone that bounds lithologic units, smaller shear zones also occur within the Maz Complex. One such meter-scale zone within Mm2 of the Maz Complex (Figs. 3 and 5C) is concentrated within metapelite and orthogneiss surrounding amphibolite. Mylonitic fabrics in this shear zone are sub-parallel to those within the Maz shear zone and asymmetric tails on garnet and staurolite porphyroblasts also indicate a sinistral sense of shear (Fig. 6B).

The Ramaditas shear zone is a broad zone of distributed deformation in the southwestern region of the Sierra de Ramaditas (Fig. 2) that strikes approximately NNE-SSW and dips steeply to the east. Mineral and stretching lineations are moderately to poorly developed, and this project did not include a systematic study of the kinematics of the shear zone. The shear zone overprints the migmatitic fabric of the paragneiss (Fig. 5D) and variably deforms the intermediate to felsic orthogneiss of the Ramaditas Complex, which suggests that the shear zone postdates peak metamorphism.

■ PETROLOGY AND THERMOBAROMETRY

The individual units within the Sierra de Maz preserve metamorphic assemblages that suggest the units experienced distinctly different metamorphic histories (Fig. 3). The Zaino Complex varies from at Chl- to St-grade, which suggests that the metamorphic conditions range from upper-greenschist to amphibolite, and the Maz Complex increases from St- to Sil+Kfs from west to east, which suggests that metamorphic grade increases from amphibolite to granulite facies. In contrast, the Taco Complex and Ramaditas Complex preserve upper amphibolite to granulite facies Sil+Kfs metapelitic assemblages. In addition, cordierite in the Ramaditas Complexes suggests the unit

Figure 5. Outcrop photographs show high-strain zones within the Sierra de Maz and Sierra de Ramaditas. (A) Mylonite and ultramylonite of the Maz shear zone developed within Grt-St-bearing schist (AT-076) of the Zaino Complex; (B) mylonite of the Maz shear zone within garnet amphibolite (AT-015) that overprints an older fabric within the amphibolite; (C) mylonite zone east of the main Maz shear zone that developed within Grt-St-bearing schist (AT-068) of the Maz Complex; and (D) mylonitic fabric of the Ramaditas shear zone that overprints earlier Kfs-Grt-Sil-Bt migmatite of the Ramaditas Complex.
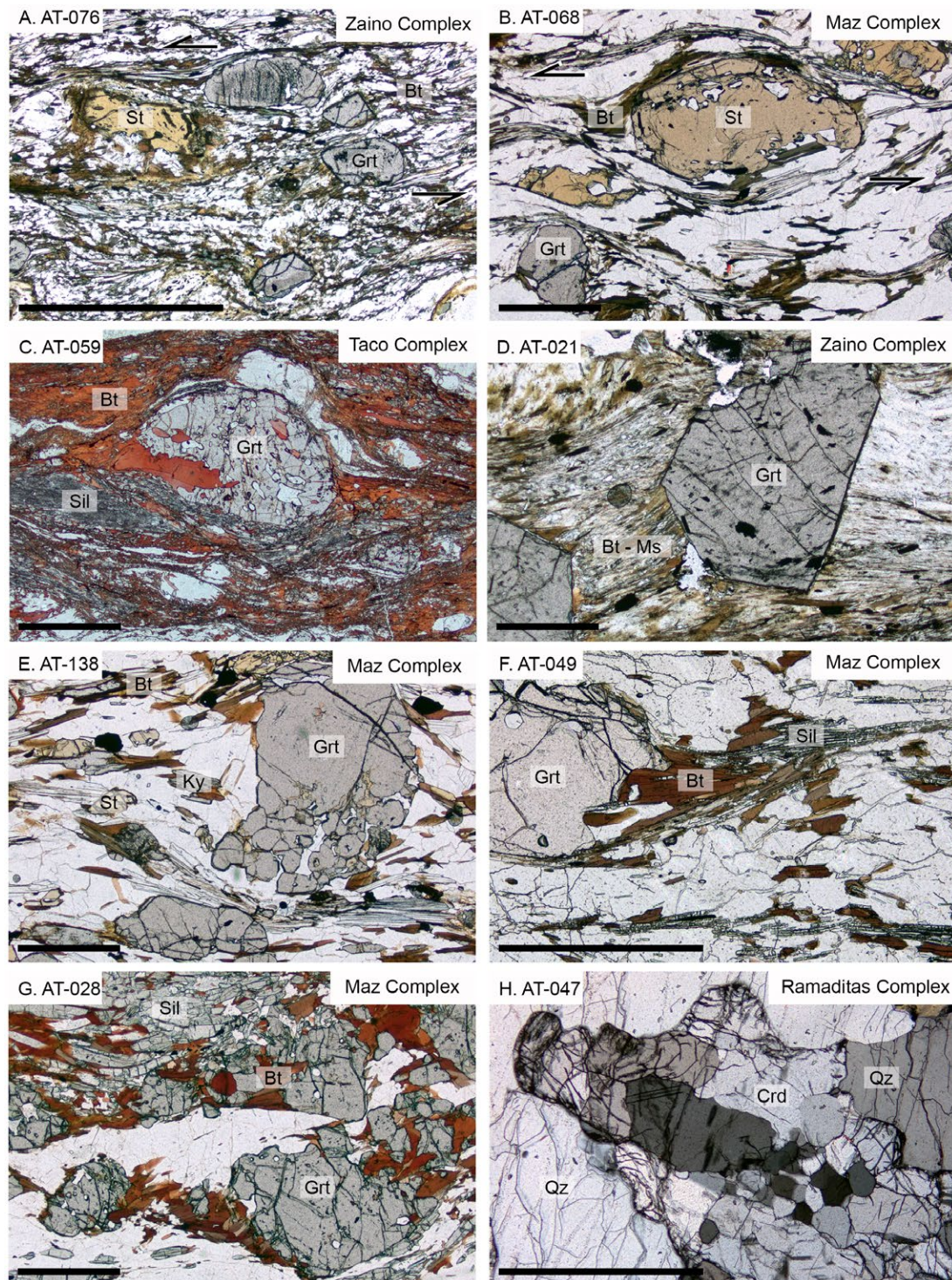
Figure 6. Photomicrographs show representative pelitic mineral assemblages from the Sierra de Maz and Sierra de Ramaditas. All thin sections were cut from samples perpendicular to foliation and parallel to lineation. (A) A St-Grt-Bt-Ms schist from the Zaino Complex shows pre-kinematic garnet with respect to the Maz shear zone and asymmetric tails on porphyroblasts that indicate a sinsitral shear sense; (B) Grt-St-Bt-Ms schist from the Mm2 member of the Maz Complex shows pre-kinematic garnet with respect to late mylonitic fabrics and asymmetric tails on porphyroblasts that indicate a sinsitral shear sense; (C) Sil-Grt-Bt ± Ms ± Kfs schist from the Taco Complex; (D) Grt-Bt-Ms schist from the Zaino Complex with post-kinematic garnet overgrowing a crenulation foliation; (E) Ky-St-Ms-Bt-Grt schist from Mm4 member of the Maz Complex; (F) Ms-Grt-Bt-Sil schist of the Mm4 member of the Maz Complex; (G) Grt-Sil-Bt-Kfs gneiss from the Mm4 member of the Maz Complex; and (H) cordierite in the leucosome of a Kfs-Grt-Bt ± Sil gneiss of the Ramaditas Complex.

may have been metamorphosed at lower pressures than the other units in the Sierra de Maz.

Samples were collected along a west-to-east transect across the Sierras de Maz and Ramaditas (Figs. 2–3) to constrain the metamorphic pressure and temperature of each unit. Representative mineral assemblages are shown in Figure 6, and additional images are provided in Figure S1[1]. Mineral compositions (Table S1; see footnote 1) were determined by electron probe microanalysis (EPMA) with a Cameca SX-100 at the University of California at Davis, California, USA, and EPMA operating conditions are reported in the Supplemental Material. Qualitative maps and quantitative transects of compositionally zoned garnet are shown in Figures S2 and S3, respectively (see footnote 1). Temperature and pressure were determined by conventional and multiequilibrium thermobarometry (Table 1). Conventional thermobarometry was performed with Grt-Bt (Ferry and Spear, 1978; Hodges and Spear, 1982) and Grt-Hbl (Graham and Powell, 1984; Perchuk et al., 1985) thermometry and Grt-Al_2SiO_5-Pl-Qz (Koziol and Newton, 1988) and Grt-Bt-Ms-Pl (Hoisch, 1990; Wu, 2015) barometry. Multiequilibrium thermobarometry was performed by the average PT method in THERMOCALC (e.g., Powell and Holland, 1994, 2010), with the assumption that water was a pure phase and using the following

solution models contained in the software AX: chlorite (Holland et al., 1998); biotite (Powell and Holland, 1999); garnet, staurolite, and muscovite (Holland and Powell, 1998); feldspar (Holland and Powell, 1992); and amphibole (Dale et al., 2000).

Pelitic protoliths within the Taco Complex contain the assemblage Sil-Grt-Bt ± Ms ± Kfs (Fig. 6C) and are locally migmatitic. Sillimanite occurs as fine acicular grains in the matrix and partly forms the foliation with biotite. Garnet porphyroblasts are wrapped by the matrix foliation (Fig. 6A), which suggests that garnet growth occurred before deformation and/or deformation outlasted garnet growth. Garnet lacks major element zoning, and the maximum X_{Mg} (0.19) composition paired with matrix Bt, Pl, and endmember Sil in sample AT-059 yielded mutltiequilibrium metamorphic conditions of 681 ± 74 °C and 6.6 ± 1.3 kbar. The estimates are consistent with the absence of observed St and the presence of Grt-Bt-Sil-Ms (Fig. 7A).

Pelitic assemblages from the Zaino Complex vary systematically from Chl, through Grt, and into St zone assemblages from west to east (Fig. 3), which is consistent with an increase in metamorphic grade across the unit. Metamorphic conditions were determined for three pelitic assemblages across the Zaino Complex (Fig. 7B). Sample AT-021 is a Grt-Bt-Ms schist with Pl, Qz, Tur,

Andrew Tholt[1], Sean R. Mulcahy[1]*, William C. McClelland[2], Sarah M. Roeske[3], Vinicius T. Meira[4], Patricia Webber[2], Emily Houlihan[2], Matthew A. Coble[5], and Jeffrey D. Vervoort[6]

[1]Geology Department, Western Washington University, Bellingham, WA, USA,
[2]Department of Geoscience, University of Iowa, Iowa City, Iowa, USA.
[3]Department of Earth and Planetary Sciences, University of California, Davis, CA, USA
[4]Department of Geology and Natural Resources, Institute of Geosciences, University of Campinas (UNICAMP), Brazil
[5]Department of Geological Sciences, Stanford University, Stanford, CA, USA
[6]School of the Environment, Washington State University, Pullman, WA, USA
*Corresponding Author

METHODS

Mineral compositions by EPMA

Mineral compositions were determined by electron probe microanalysis (EPMA) with a Cameca SX-100 at UC Davis. All minerals were analyzed with an accelerating voltage of 15 kV but with variable current (nA) and spot sizes (μm) depending on the mineral as follows: garnet (20 nA, 1 μm); feldspar (10 nA, 10 μm); biotite (10 nA, 5 μm); muscovite (7 nA, 10 μm); and amphibole (10 nA, 1 μm). Matrix corrections were performed with the ZAF method. Mineral compositions used for thermobarometry are listed in Table S1.

Garnet trace element compositions by LA-ICP-MS

Rim to rim trace element concentrations were determined by laser ablation inductively coupled plasma mass spectrometry (LA-ICPMS) in the AMSEC facilities at Western Washington University using an Agilent 7500ce ICPMS with a New Wave UP-213AS laser ablation accessory utilizing a 213nm UV Nd:YAG class IV laser. Time-resolved spectra with a 1 ms integration were collected using a 55 μm diameter spot size. Working acquisition time was 120 seconds, including 30 seconds of background, and 90 seconds of sample ablation. All analyses

TABLE 1. METAMORPHIC CONDITIONS OF THE SIERRAS DE MAZ AND RAMADITAS

Sample	Latitude (°N)	Longitude (°W)	Assemblage +Qz	Index mineral	Conventional thermobarometry Temperature (°C)	Pressure (kbar)	Multiequilibrium thermobarometry Temperature (°C)	±2σ	Pressure (kbar)	±2σ	cor	σ_fit	fit
Taco Complex													
AT-059	−29.4671	−68.4926	Grt-Sil-Bt-Plg±Ms±Kfs	Sil	651	6.8	681	74	6.6	1.3	0.746	0.20	1.96
Zaino Complex													
AT-021a	−29.1932	−68.5136	Grt-Bt-Ms-Plg-Kfs	Grt	486	7.1	512	50	7.4	1.7	0.893	2.15	1.96
AT-017	−29.1905	−68.4936	Grt-Bt-Ms-Plg-Chl	Grt	550	7.4	555	25	7.9	0.7	0.329	0.84	1.61
AT-076*	−29.2011	−68.4732	Grt-Bt-Ms-Plg-St	St	645	7.5	640	46	7.0	1.8	0.738	1.63	1.73
Maz Complex													
AT-015*	−29.1886	−68.4740	Grt-Bt-Plg-Amp	–	548	–	574	95	7.5	1.2	0.860	1.47	1.61
AT-079	−29.1882	−68.4612	Grt-St-Bt-Ms-Plg-Chl	St	557	7.1	643	46	7.1	1.1	0.502	0.59	1.61
AT-068*	−29.1861	−68.4570	Grt-St-Bt-Ms-Plg	St	637	6.7	632	45	7.2	1.0	0.506	0.58	1.61
AT-070	−29.1869	−68.4545	Grt-St-Bt-Ky-Ms-Plg-Chl	Ky	599	7.2	615	13	7.0	1.7	0.068	0.62	1.49
AT-083	−29.1882	−68.4464	Grt-St-Ky-Bt-Ms-Plg	Ky	607	7.6	622	68	7.1	1.4	−0.315	1.38	1.73
AT-044	−29.2140	−68.3780	Grt-Sil-Bt-Plg-Kfs	Sil-Kfs	729	–	757	40	6.9	1.2	0.790	1.67	1.73
AT-028	−29.2216	−68.3674	Grt-Sil-Bt-Plg-Kfs	Sil-Kfs	749	8.0	869	70	7.8	1.0	0.625	1.23	1.61
Ramaditas Complex													
AT-047	−29.2867	−68.2835	Grt-Bt-Plg-Cd	Crd	766	5.1	850	70	5.5	1.5	0.762	0.70	1.61

*Sample located within mylonite/ultramylonite zone.

Note: For conventional thermobarometry the assumed 2σ uncertainties on temperature and pressure are ± 50 °C and ± 1 kbar, respectively. For multiequilibrium thermobarometry, cor is the correlation between the uncertainties in pressure and temperature and defines the shape and orientation of the error ellipse, σ_fit is measure of the goodness of fit equal the √ (MSWD), fit is the maximum allowable value of σ_fit from a χ² test at the 95% confidence level (Powell and Holland, 1994). Sample AT-015 is a mafic protolith so no index mineral is listed. Pressures for samples AT-015 and AT-044 were not determined by conventional thermobarometry. The dash indicates that there was either no index mineral in the assemblage or no pressure was determined.
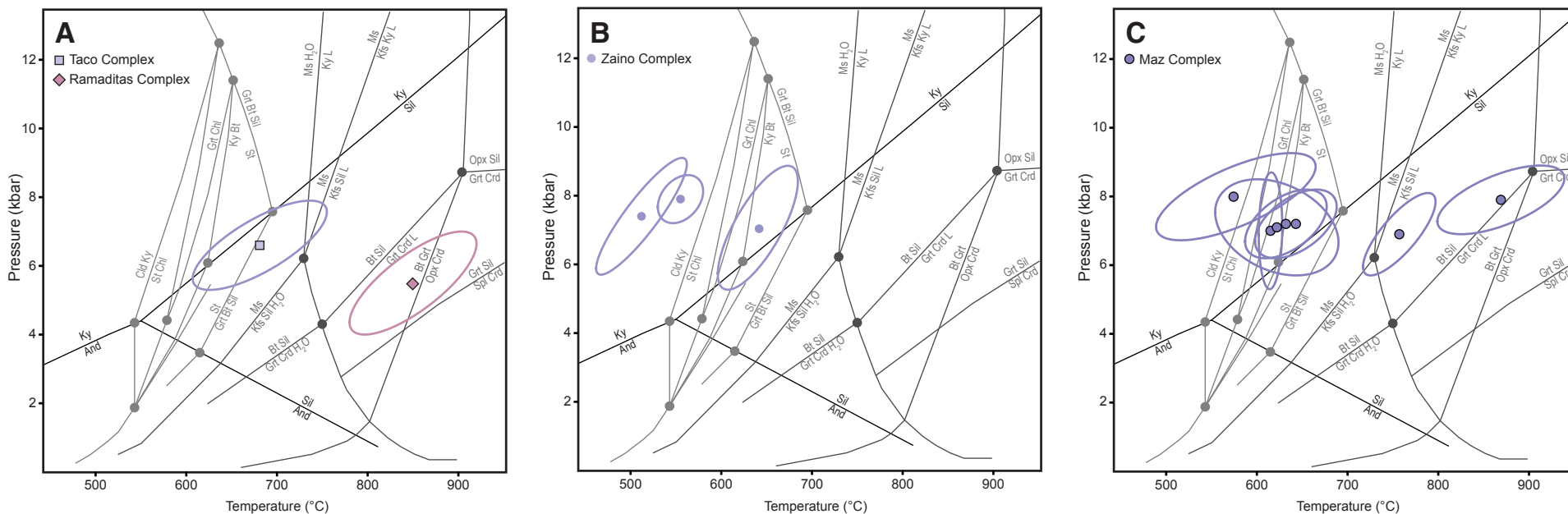
Figure 7. Pressure-temperature diagram plots of metamorphic conditions in the Sierra de Maz. Individual diagrams show the results of the multiequilibrium thermobarometry (Table 1) for (A) the Taco and Ramaditas Complexes; (B) the Zaino Complex; and (C) the Maz Complex. The diagrams have petrogenetic grids for metapelites in the KFMASH system at melt-absent (light gray; Spear and Cheney, 1989) and melt-present (dark gray; Spear et al., 1999) conditions. For comparison, Figure S4 (see text footnote 1) plots both the conventional and mutliequilibrium thermobarometry results.

and Opq (Fig. 6D). Garnet prophyroblasts contain inclusions of Chl and Czo that are less abundant to absent in the matrix, which suggests that garnet formed via reactions involving the breakdown of these minerals. The sample has two foliations; the first is defined by alternating mica-rich and quartzo-feldspathic layers, and the second is an axial planar cleavage. Both foliations are truncated by euhedral garnet (Fig. 6D), which suggests that garnet growth postdated or outlasted foliation development. Garnet is compositionally zoned with a bell-shaped X_{Sps} profile that decreases from 0.13 to 0.01 and X_{Mg} concentrations that increase from 0.08 to 0.13 core to rim, which is suggestive of a single phase of prograde garnet growth. Garnet rim compositions, paired with matrix Ms, Bt, and Pl in contact with garnet, record metamorphic conditions of 512 ± 50 þC and 7.4 ± 1.7 kbar. Sample AT-017 is a Grt-Bt-Chl-Ms schist with Pl, Qz, and Ap. Subhedral to euhedral garnet porphyroblasts are wrapped by the external mica foliation and are partially resorbed. Garnet locally preserves a faint internal foliation defined by quartz inclusions aligned at a high angle to the matrix foliation, which suggests that garnet growth predated foliation development. Chlorite is intergrown with matrix biotite and muscovite and is part

of the peak metamorphic assemblage. Metamorphic conditions for the garnet and matrix assemblage are 555 ± 25 þC and 7.9 ± 0.7 kbar. Sample AT-076 is a St-Grt-Bt-Ms schist with Pl, Qz, Tur, and minor retrograde Chl (Fig. 6A) from within the highest strain portion of the Maz shear zone (Fig. 5A). Both St and Grt porphyroblasts are wrapped by the mylonitic fabric. Garnet has abundant inclusions of Qz and opaques in the core that are aligned at a high-angle to the external foliation and relatively inclusion-free rims (Fig. 6A), which suggests that garnet growth predates deformation at the Maz shear zone. The garnet cores and rims are uniform in composition but distinct from one another. The garnet cores have higher X_{Sps} = 0.11 and lower X_{Grs} = 0.05 than the garnet rims with X_{Sps} = 0.06 and X_{Grs} = 0.07. Garnet rim compositions, combined with St and matrix Bt, Ms, and Pl in contact with garnet, record metamorphic conditions of 640 ± 46 þC and 7.0 ± 1.8 kbar. The calculated metamorphic conditions of the three samples are consistent with observed variation in index minerals across the Zaino Complex from Chl-Grt (±Ctd) up through St (Fig. 7B).

Pelitic assemblages from the Maz Complex vary systematically from St, through Ky, and into Sil-Kfs zone assemblages from west to east (Figs. 3 and

6B, 6E, and 6F); this is consistent with an increase in metamorphic grade across the unit from amphibolite to granulite facies. Metamorphic conditions were determined for pelitic assemblages across the Maz Complex (Table 1), although more samples were analyzed in Mm1 and Mm2 because suitable assemblages are not as common in Mm3 and Mm4. Sample AT-015 is a Bt-Grt amphibolite within the Maz shear zone. Amphibole is ferro-pargasite that together with Bt and alternating layers rich in Qz and Plg define the mylonitic foliation. Small sub- to anhedral garnet cores have higher $X_{Sps} = 0.0.37$ and lower $X_{Alm} = 0.65$ than garnet rims with $X_{Sps} = 0.025$ and $X_{Alm} = 0.70$. Metamorphic conditions for the sample are 574 ± 95 °C and 7.5 ± 1.2 kbar. Sample AT-068 from within a high strain zone in the Mm2 member of the Maz Complex (Fig. 5C) contains the assemblage Grt-St-Bt-Ms-Pl-Qz (Fig. 6B). Staurolite and garnet porphyroblasts are wrapped by the mylonitic foliation, which suggests that both phases grew prior to deformation and/or that deformation outlasted porphyroblast growth. Staurolite has a uniform composition with $X_{Mg} = 0.15$, and garnet has irregular major element zoning with elevated $X_{Sps} = 0.04$ and $X_{Grs} = 0.06$ near the garnet rim and along fractures; X_{Mg} decreases from 0.16 near core to 0.12 at the rim. Garnet compositions with maximum X_{Mg} paired with matrix St, Bt, Ms, and Pl yielded metamorphic conditions of 632 ± 45 °C and 7.2 ± 1.0 kbar. Sample AT-028 from the Mm4 member of the Maz Complex contains the pelitic granulite assemblage Grt-Sil-Bt-Kfs-Pl-Qz ± Rt (Fig. 6G). Sillimanite occurs as large prismatic grains in the matrix, and kyanite is locally found as inclusions in garnet. Garnet lacks major element zoning except for weakly zoned X_{Mg} that decreases from 0.29 in the core to 0.25 at the rim. Garnet maximum X_{Mg} compositions, paired with matrix Bt, Kfs, and Pl in contact with garnet, yielded metamorphic conditions of 869 ± 70 °C and 7.8 ± 1.0 kbar, which is consistent with the presence of Sil+Kfs in the sample (Fig. 7C) and migmatite within the unit.

Migmatitic metapelites from the Ramaditas Complex contain the low- to medium-pressure granulite facies assemblage Kfs-Grt-Bt ± Sil ± Crd. Sample AT-047 contains Crd (Fig. 6H) and lacks Sil. Garnet X_{Sps} content increases from 0.04 to 0.07 and X_{Mg} decreases from 0.23 to 0.17 from core to rim, which is indicative of retrograde diffusion from high temperatures (e.g., Tuccillo et al., 1990; Florence and Spear, 1995), and corderite is not zoned with an $X_{Mg} = 0.92$. Garnet maximum X_{Mg} compositions, paired with matrix Bt, Crd, Kfs, and Pl in contact with garnet, yielded metamorphic conditions of 850 ± 70 °C and 5.5 ± 1.5 kbar, which plots within the Bt-Grt-Sil-Crd stability field (Fig. 7A).

■ GEOCHRONOLOGY

Garnet Lu-Hf Geochronology

We measured garnet Lu-Hf isotope data from samples across the Sierra de Maz to date the timing of metamorphism and deformation. Garnet and matrix (garnet-free whole rock) separates were analyzed from six different samples. Sample Lu-Hf chemistry and isotopic analysis using the Thermo-Finnigan NEPTUNE were performed at Washington State University. Dissolution procedures followed Mulcahy et al. (2014). Garnet rare earth element concentrations and zoning profiles of garnet listed in Table S2 are shown in Figures S5–S6 (see footnote 1). Garnet isotopic data are in Table S2, and the results are plotted in Figure 8 and summarized in Table 2. Garnet Lu-Hf isochron ages and εHf values were calculated using a ^{176}Lu decay constant value of 1.867×10^{-11} a^{-1} (Scherer et al., 2001; Söderlund et al., 2004) and ^{176}Hf/^{177}Hf = 0.282785 and ^{176}Lu/^{177}Hf = 0.0336 for chondrite uniform reservoir (CHUR) (Bouvier et al., 2008). Uncertainties are reported as 2σ unless the mean square of weighted deviates (MSWD) exceeds the expected mean value for the given number of analyses; in that case, the uncertainties are expanded by the √MSWD (Fig. 8).

Garnet from two samples within the Zaino Complex record a single episode of Silurian metamorphism. Sample AT-021 was collected within the garnet zone of the Zaino Complex (Fig. 3). Lutetium is concentrated within the cores of garnet porphyroblasts and decreases toward the rim consistent with a single generation of garnet growth (Fig. S6). Garnet has a bimodal grain size with grains either larger than 2 mm or between 1 mm and 2 mm, and the smaller grain size fraction had elevated ^{176}Lu/^{177}Hf in comparison with the larger garnet. The sample yielded an age of 422 ± 9.6 Ma (MSWD = 4.6; Fig. 8A), and the Mn and Lu zoning profiles and high MSWD are consistent with a single period of protracted garnet growth (Kohn, 2009). Sample AT-076 was collected within the staurolite zone of the Zaino Complex and within the highest strain portion of the Maz shear zone. The trace element profile shows that Lu is concentrated in the garnet rims (Fig. S6), which implies that the age is biased toward the later stages of garnet growth. The sample produced an isochron age of 427 ± 4.5 Ma (MSWD = 0.8; Fig. 8B).

Three samples within the Maz Complex show a complex metamorphic history. Sample AT-015 is a garnet amphibolite within the Mm1 unit of the Maz Complex and is from the high strain fabric of the Maz shear zone that overprints an older fabric within the Maz Complex. The small (<100 um) subhedral garnet overgrows the mylonitic foliation defined by aligned amphibole, which suggests that garnet growth outlasted deformation. The sample yielded an age of 427.2 ± 6.3 Ma (MSWD = 5.6; Fig. 8C). Sample AT-068 occurs within a mylonite zone within the Maz Complex. Lutetium is elevated in the garnet core but also increases at intermittent points toward the rim (Fig. S6). Ages between individual garnet separates and the matrix separates scatter between 759 Ma and 591 Ma (Fig. 8D). Sample AT-028 is a Sil-Kfs-Grt-Bt gneiss along the eastern margin of the Maz Complex. Garnet cores have elevated Lu concentrations compared to garnet rims (Fig. S6). Ages between individual garnet separates and the matrix separates scatter between 1074 Ma and 1031 Ma (Fig. 8D). The scatter in garnet separates on isochrons from samples within Mm2 (AT-068) and Mm4 (AT-028) suggests that the Maz Complex records a polymetamorphic history or experienced diffusive loss of Hf after initial garnet growth.

A sample from the Ramaditas Complex (AT-047) records peak metamorphism of Grt-Sil-Bt gneiss in the Ordovician with evidence for a younger metamorphic event. Garnet cores have two central peaks that decrease asymmetrically toward each rim (Fig. S6). Two garnet separates and the matrix
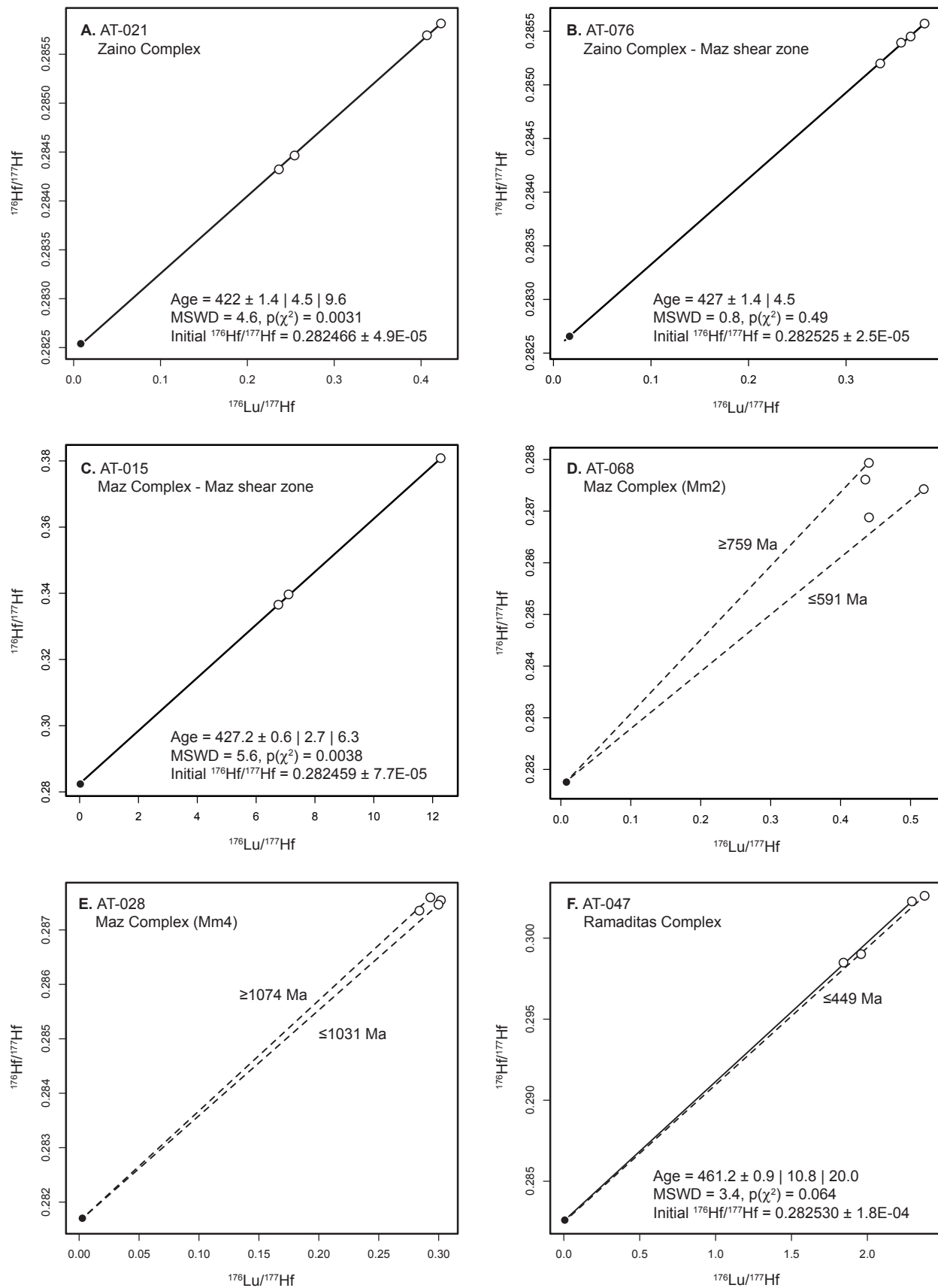
Figure 8. Garnet Lu-Hf isochrons are shown. (A) Garnet and (B) staurolite-grade pelitic schist from the Zaino Complex; (C) garnet amphibolite; (D) staurolite-grade pelitic schist; (E) Sil-Kfs–bearing migmatitic gneiss from the Maz Complex; and (F) Grt-Crd–bearing migmatitic gneiss from the Ramaditas Complex. White circles are garnet separates and black circles are matrix separates. The results are reported as t ± x | y | z, where t is the isochron age, x is the standard error, y is the 95% confidence interval, and z is the confidence interval for t with overdispersion calculated as z = y√MSWD (Vermeesch, 2018).

TABLE 2. SUMMARY OF DATES FROM THE
SIERRAS DE MAZ AND RAMADITAS

Sample	Latitude (°N)	Longitude (°W)	Mineral	Age	2σ
Taco Complex					
AT-059	–29.46714	–68.49264	Monazite	467.7	2.9
Zaino Complex					
AT-021a	–29.19322	–68.51361	Garnet	422.0	9.6
AT-076	–29.20108	–68.47318	Garnet	427.0	4.5
			Monazite	418.7	3.6
Maz Complex					
AT-015	–29.18856	–68.47404	Garnet	427.2	6.3
AT-068	–29.18615	–68.45705	Monazite	1214.5	37.0
			Monazite	409.9	2.3
AT-028	–29.22158	–68.36735	Monazite	1227.0	7.5
			Monazite	413.2	7.1
Ramaditas Complex					
AT-047	–29.28666	–68.28350	Garnet	461.2	10.8
			Monazite	461.6	3.9
			Monazite	426.1	11.4

define an isochron with an oldest age of 461.2 ± 10.8 Ma (MSWD = 3.4), and two younger fractions imply a younger metamorphic event post 449 Ma (Fig. 8F).

Monazite U-Pb Geochronology

We dated monazite from samples across the Sierra de Maz to determine the timing of metamorphism and deformation and interpret the cause of scatter in some of the garnet Lu-Hf isochrons. Monazite U-Th-Pb analysis was conducted in situ by sensitive high-resolution ion microprobe-reverse geometry (SHRIMP-RG) co-operated by the U.S. Geological Survey and Stanford University in the Stanford University–U.S. Geological Survey Micro Analysis Center at Stanford University. The analytical methods, back-scattered electron (BSE) images of the dated monazite grains (Figs. S7–S11 [see footnote 1]), and trace element concentrations (Fig. S12) and isotopic data for monazite U-Pb analyses (Table S4; see footnote 1) are provided in the Supplemental Material. Uncertainties are reported as 2σ unless the MSWD exceeds the expected mean value for the given number of analyses, in which case the uncertainties are expanded by the √MSWD (Figs. 9–10 and Table 2).

One sample from the Taco Complex (Fig. 2) records peak Ordovician metamorphism with evidence of younger metamorphism and deformation. Monazite in sample AT-059, a Kfs-Sil-Grt-Bt schist, occurs as rounded inclusions that lack zoning in garnet and as elongate grains in the matrix aligned parallel to the foliation that locally contain inclusions of sillimanite (Fig. S7). Most of the monazite grains in the matrix are weakly zoned with BSE bright cores

and dark rims (Fig. S7). Concordant monazite ages range from ca. 490 Ma to 420 Ma (Fig. 9A). Monazite inclusions in garnet and the cores of large monazite grains in the matrix have a ^{207}Pb-corrected ^{206}Pb/^{238}U weighted mean age of 467.7 ± 4.3 Ma (MSWD = 2.1, Fig. 10A), while several monazite rims and small monazite grains in the matrix range down to ca. 420 Ma.

Monazite in Zaino Complex sample AT-076 within the Maz shear zone occurs as elongate grains aligned within the mylonitic foliation, and no monazite grains were observed as inclusions within garnet. Monazite BSE images show patchy and somewhat irregular zoning of BSE-light and BSE-dark regions (Fig. S8). Concordant monazite ages ranged from 420 Ma to 402 Ma (Fig. 9B), and despite the different zoning there were no statistically distinguishable age populations. A ^{207}Pb-corrected ^{206}Pb/^{238}U weighted mean age of all monazite grains yielded an age of 418.7 ± 3.6 Ma (MSWD = 1.1; Fig. 10B).

Monazite samples from the Maz Complex record separate Proterozoic and Devonian metamorphic events. Sample AT-068 occurs within a mylonite-ultramylonite zone east of the main Maz shear zone. Monazite is generally unzoned or patchily zoned (Fig. S9) and occurs as inclusions in both garnet and staurolite and as elongate grains aligned within the mylonitic foliation. Matrix monazite and monazite inclusions along fractures in garnet and staurolite are concordant and range in age from 432 Ma to 380 Ma, while a single grain of monazite within unfractured garnet preserved an oscillatory-zoned core and was discordant (Fig. 9C). A discordia line fit to the data produced a lower intercept age of 407.8 ± 7.9 Ma and an upper intercept of 1214.5 ± 37.0 Ma (Fig. 9C). Matrix grains yielded a ^{207}Pb-corrected ^{206}Pb/^{238}U weighted mean age of 409.9 ± 3.7 Ma (MSWD = 2.6; Fig. 10C).

Sample AT-028 is a Kfs-Grt-Sil-Bt gneiss near the eastern edge of the Sierra de Maz. Monazite occurs as elongate grains within the matrix of the foliation and as coarse inclusions in garnet of up to 200 microns in length. Monazite grains have variable BSE zoning patterns that consist of bright, oscillatory-zoned cores; patchy overgrowths commonly formed around cores; and dark rims on matrix grains (Fig. S10 [footnote 1]). Regression of all monazite analyses on a concordia diagram resulted in an upper intercept age of 1234.7 ± 10.1 Ma and a lower intercept age of 400.5 ± 16.4 Ma (Fig. 9D). Concordant upper intercept ages from monazite in garnet and BSE bright cores in matrix monazite ranged from 1191 Ma to 1262 Ma and produced a ^{204}Pb-corrected ^{207}Pb/^{206}Pb weighted mean age of 1227.1 ± 7.5 Ma (MSWD = 1.5; Fig. 10D). Concordant lower intercept ages of BSE dark rims on bright cores ranged from 397 Ma to 431 Ma and have a ^{207}Pb-corrected ^{206}Pb/^{238}U weighted mean age of 413.2 ± 19.7 Ma (MSWD = 7.7; Fig. 10E).

Monazite in the Ramaditas Complex records Ordovician metamorphism with a Silurian–Devonian metamorphic and/or deformation event. Sample AT-047 is a Kfs-Grt-Bt ± Crd gneiss and monazite that occurs as inclusions in garnet and as rounded grains in the matrix with complex or oscillatory zoned cores with BSE bright and dark rims (Fig. S11 [footnote 1]). Monazite is concordant and ranges in age from 418 Ma to 472 Ma (Fig. 9E). Monazite in garnet and the cores of matrix monazite have a ^{207}Pb-corrected ^{206}Pb/^{238}U weighted mean age of 461.6 ± 3.9 Ma (MSWD = 1.6; Fig. 10F). Rims on older
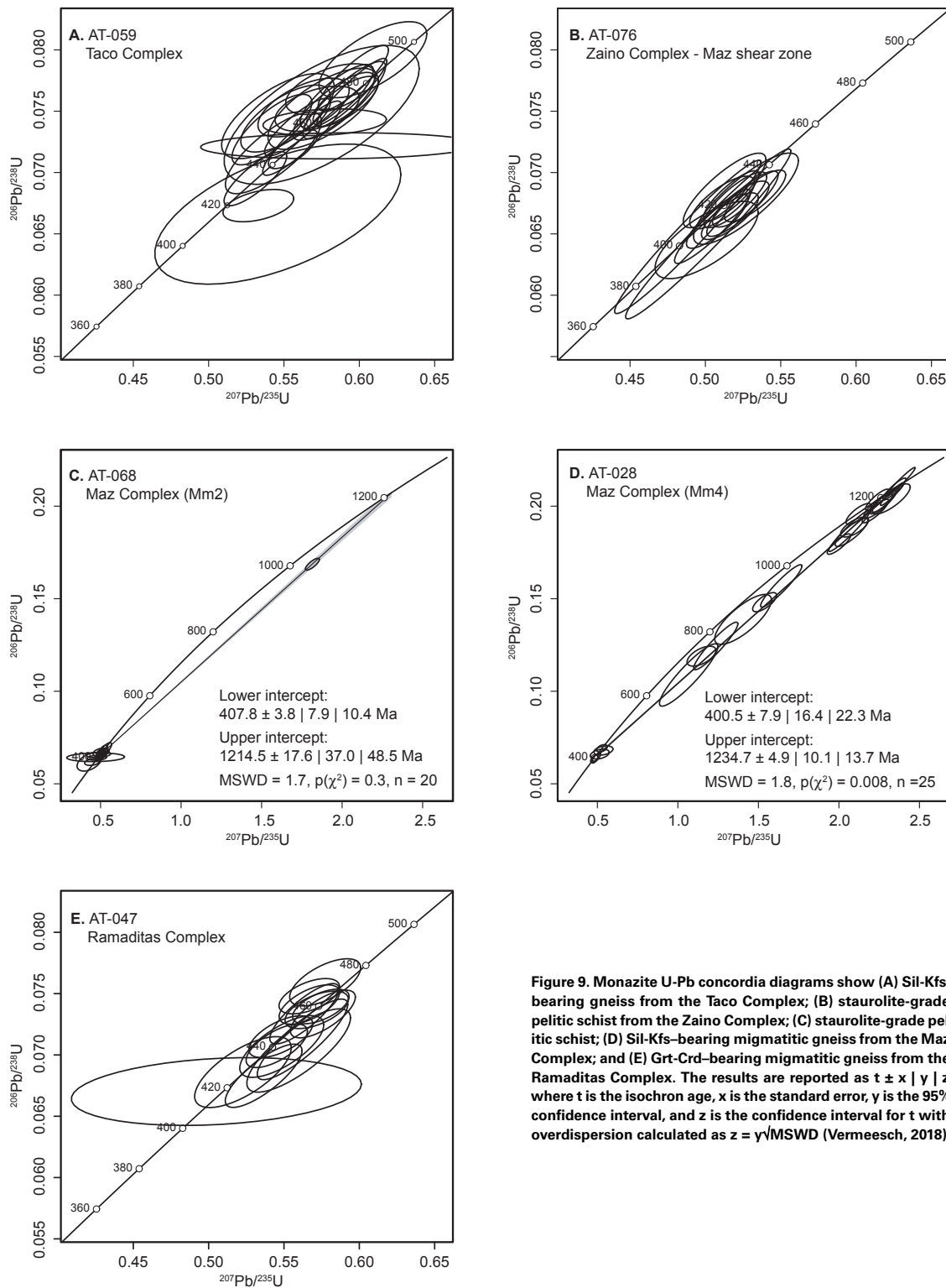
Figure 9. Monazite U-Pb concordia diagrams show (A) Sil-Kfs–bearing gneiss from the Taco Complex; (B) staurolite-grade pelitic schist from the Zaino Complex; (C) staurolite-grade pelitic schist; (D) Sil-Kfs–bearing migmatitic gneiss from the Maz Complex; and (E) Grt-Crd–bearing migmatitic gneiss from the Ramaditas Complex. The results are reported as t ± x | y | z, where t is the isochron age, x is the standard error, y is the 95% confidence interval, and z is the confidence interval for t with overdispersion calculated as z = y√MSWD (Vermeesch, 2018).
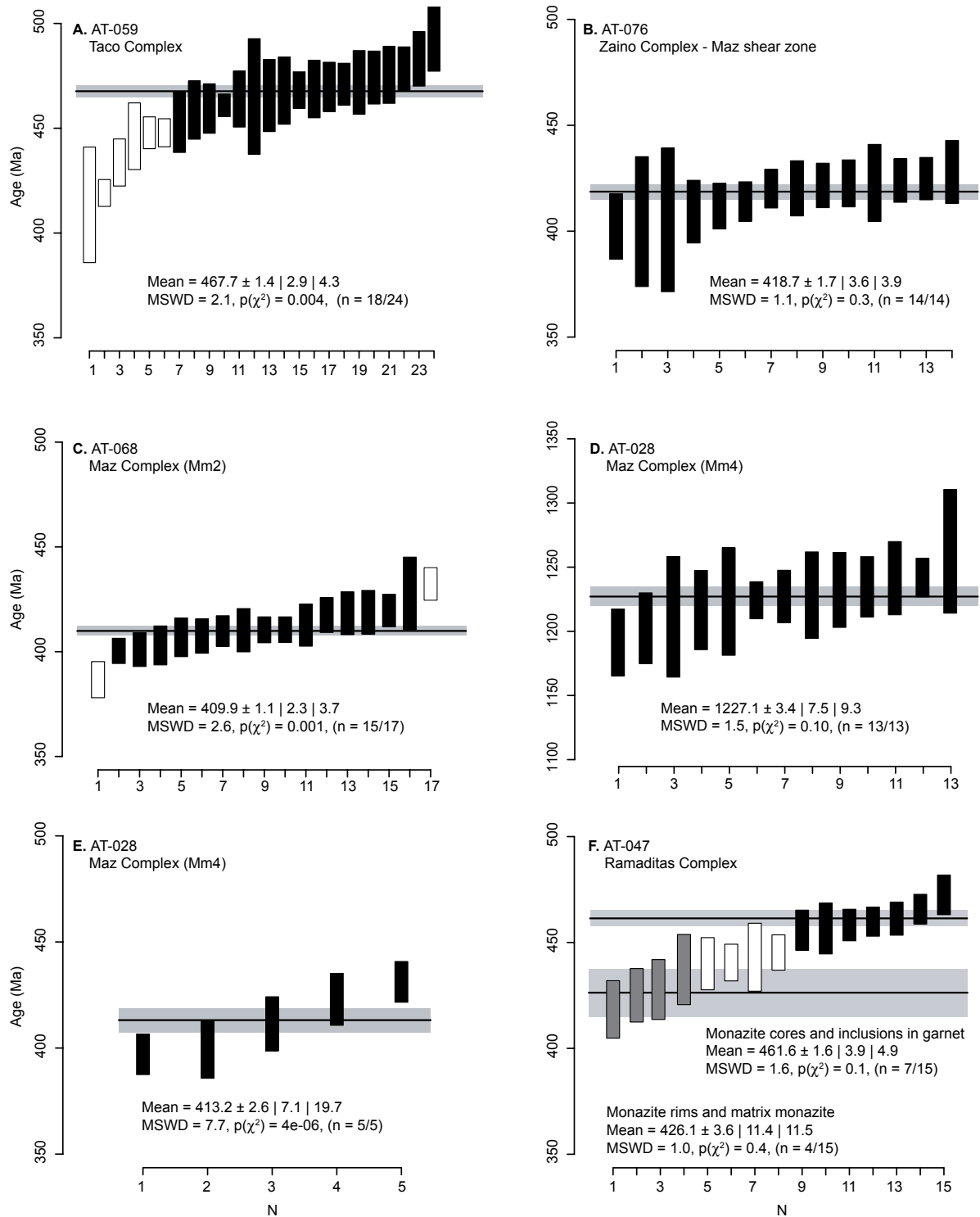
Figure 10. Monazite U-Pb weighted mean ages are shown. (A) Sil-Kfs–bearing gneiss from the Taco Complex; (B) staurolite-grade pelitic schist from the Zaino Complex; (C) staurolite-grade pelitic schist from the Maz Complex; (D) Monazite in garnet and BSE bright cores in matrix monazite from Sil-Kfs–bearing migmatitic gneiss from the Maz Complex; (E) BSE dark monazite rims on matrix monazite from Sil-Kfs–bearing migmatitic gneiss from the Maz Complex; and (F) Grt-Crd–bearing migmatitic gneiss from the Ramaditas Complex. For A–C and E–F, the ages are [207]Pb-corrected [206]Pb/[238]U ages and for D the ages are [204]Pb-corrected [207]Pb/[206]Pb ages. The results are reported as t ± x | y | z, where t is the isochron age, x is the standard error, y is the 95% confidence interval, and z is the confidence interval for t with overdispersion calculated as z = y√MSWD (Vermeesch, 2018).

matrix monazite define a [207]Pb-corrected [206]Pb/[238]U weighted mean age of 426.1 ± 11.4 Ma (MSWD = 1.0; Fig. 10F). Four analyses produced intermediate ages that we interpret as variably mixed core and rim domains.

■ DISCUSSION

The metamorphic conditions and ages of metapelites within the Sierra de Maz suggest that each unit—the Taco Complex, the Zaino Complex, the Maz Complex, and the Ramaditas Complex—experienced distinctly different metamorphic conditions and/or were metamorphosed at different times (Fig. 11). These differences, when combined with existing data, place new constraints on the correlation of the units with one another and within the region (Fig. 12). In addition, evidence for a component of strike-slip deformation during the Siluran–Devonian (ca. 427–410 Ma) within the Western Sierras Pampeanas suggests a fundamental change in the tectonic setting of the Famatina margin at that time.

The Taco Complex, as exposed in the southwestern corner of the Sierra de Maz (Fig. 2), experienced Ordovician, medium-pressure upper amphibolite facies metamorphism with continued or later metamorphism and deformation into the Silurian. The Sil+Kfs metapelites in the Taco Complex record peak metamorphism at ~6.5–7 kbar and 680 °C (Fig. 7A). Monazite ages from the same metapelite constrain the timing of peak metamorphism at 468 ± 4 Ma and either a younger event or continued metamorphism and deformation down to ca. 420 Ma (Figs. 10–11). Lucassen and Becchio (2003) reported titanite ages of 531 ± 16 Ma, 443 ± 3 Ma, and several grains with ages down to 415–340 Ma from the same region of the Taco Complex that they interpreted to record prolonged

high-temperature metamorphism. The ca. 531 Ma titanite age overlaps in error with amphibole [40]Ar/[39]Ar ages of ca. 515 Ma in the Sierra de Pie de Palo (Mulcahy et al., 2007); if valid, these ages suggest there may be an older but not yet characterized Cambrian metamorphic event within the Taco Complex.

The Zaino and Maz Complexes preserve a Barrovian metamorphic sequence that increases in metamorphic grade west to east from the chlorite (<500 °C) up through the sillimanite+K-feldspar zone (>800 °C) (Figs. 3 and 7), consistent with the observations of previous workers that metamorphic grade increases across the range (e.g., Kilmurray and Dalla Salda, 1971; Casquet et al., 2008b). The Zaino Complex experienced a single episode of greenschist- to amphibolite-facies metamorphism (Fig. 11) recorded by Chl- and rare Ctd-bearing metapelites in the west and Grt- and St-bearing metapelites in the east, adjacent to the Maz shear zone (Figs. 6A and 6D). Metamorphic pressures are roughly uniform at ~7 kbar, and temperature increases west to east from ~512 °C to ~640 °C (Fig. 7B). Garnet Lu-Hf and monazite U-Pb ages within the Zaino Complex are Silurian and range from 427 ± 5 Ma to 419 ± 4 Ma (Figs. 8 and 10) and constrain the timing of prograde to peak metamorphism within the Zaino Complex.

In contrast, the Maz Complex records at least two distinct episodes of high-grade metamorphism. The metamorphic grade within metapelites of the Maz Complex increases from the staurolite zone in the Maz shear zone in the west up through the sillimanite+K-feldspar zone along the eastern range front of the Sierra de Maz (Fig. 3). Pressure within the Maz Complex is generally uniform between 7 kbar and 8 kbar, but temperatures increase from west to east from ~575 °C to 850 °C (Fig. 7C), consistent with the occurrence of migmatite in the highest-grade portions of the unit. Garnet throughout the Maz Complex is dominantly pre-kinematic with respect to the prominent foliation. Garnet
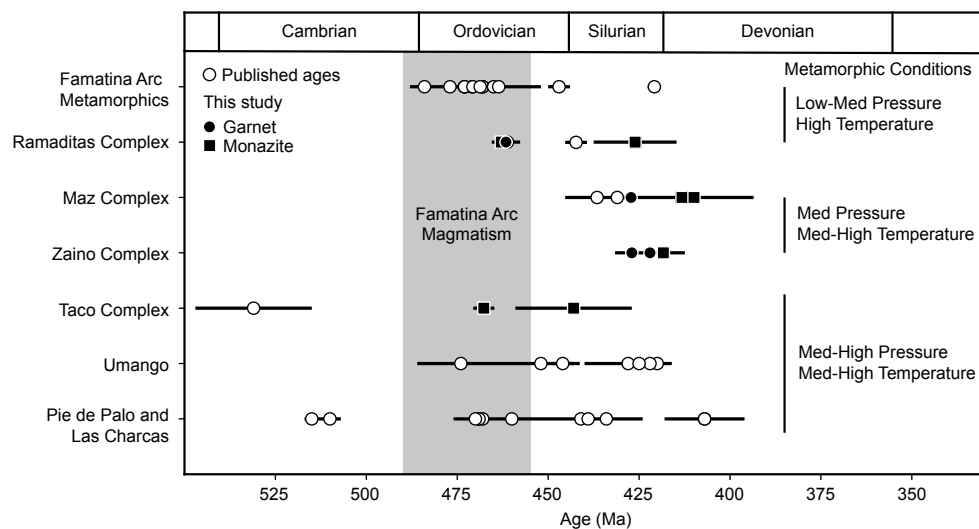

Figure 11. Timing of Proterozoic metamorphism in the Western Sierras Pampeanas is plotted. The diagram includes garnet (Lu-Hf, Sm-Nd) and monazite, titanite, and zircon (U-Pb) ages reported from metamorphic assemblages in the region. Points are absolute reported ages; the black bars span the overlapping uncertainties of the reported ages. The relative metamorphic conditions for each region are also described (see text for details). Published data shown in the diagram are from: Grissom et al. (1998); Casquet et al. (2001, 2008b); Lucassen and Becchio (2003); Galindo et al. (2004); Büttner et al. (2005); Rapela et al. (2005); Steenken et al. (2006); Mulcahy et al. (2007, 2011, 2014); Gallien et al. (2010); Lucassen et al. (2010); and Finch et al. (2017).
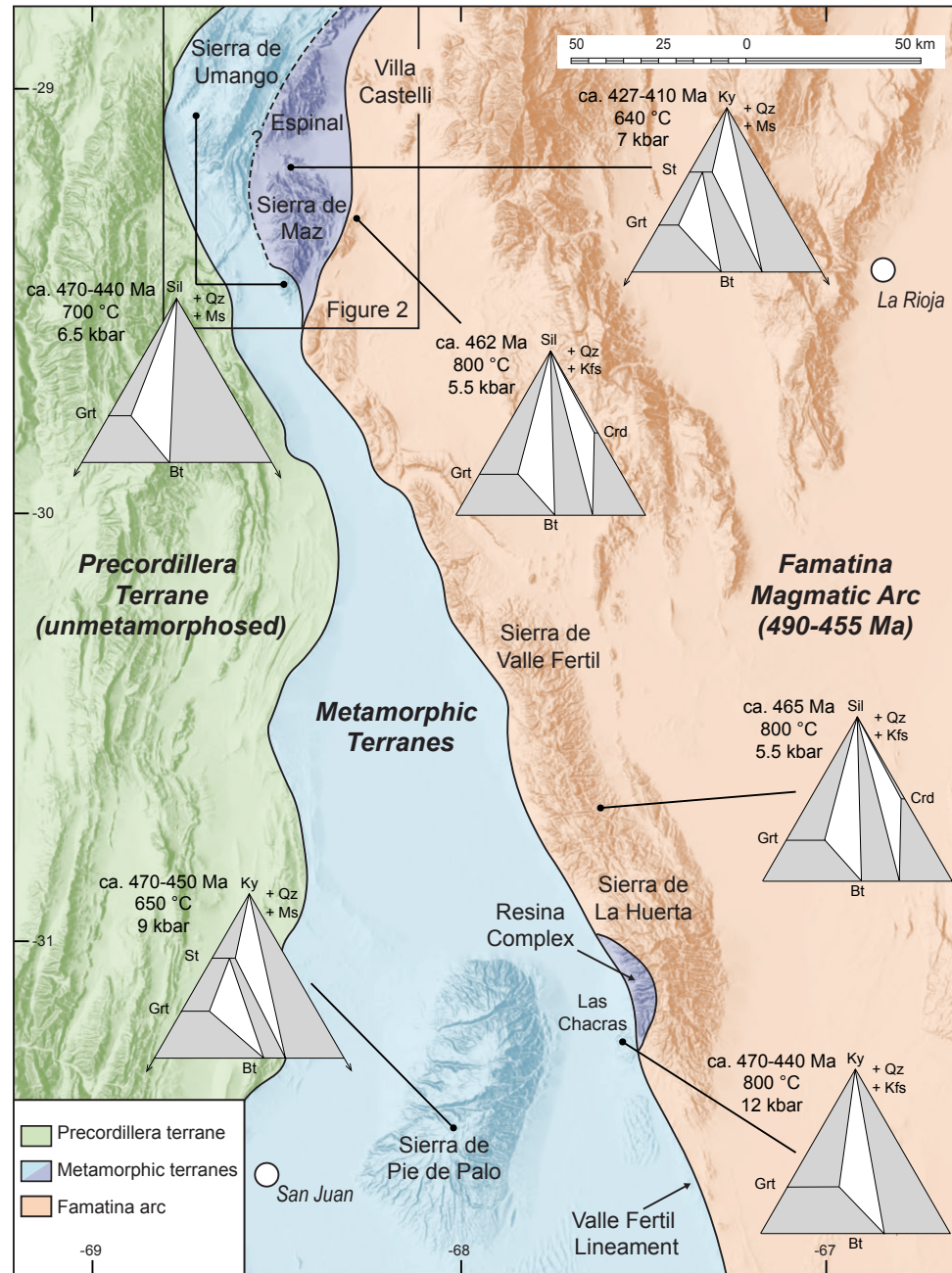
Figure 12. This revised tectonic map of the Western Sierras Pampeanas proposes new boundaries between the Zaino, Maz, and Resina Complexes (purple) of the MARA terrane and other metamorphic terranes of the Western Sierras Pampeanas (blue) based on the timing of conditions of metamorphism. Pseudo-AFM diagrams for regions discussed were constructed with the software Theriak-Domino (de Capitani and Petrakakis, 2010). Pressure-temperature conditions for the AFM diagrams plotted on the figure are from this study and the following references: Otamendi et al. (2008); Lucassen et al. (2010); Mulcahy et al. (2011, 2014); Varela et al. (2011); Tibaldi et al. (2013); Alasino et al. (2014); and Ramacciotti et al. (2019b).

Lu-Hf and monazite U-Pb ages date two different metamorphic events within the Maz Complex: an older Proterozoic metamorphic event at 1227 ± 8 Ma and a younger Paleozoic metamorphic and/or deformation event(s) between 427 ± 6 Ma and 410 ± 4 Ma. Proterozoic monazite inclusions in garnet are consistent with previously published ages for ca. 1.2 Ga metamorphism within the Maz Complex (Casquet et al., 2001; Lucassen and Becchio, 2003). The age of garnet within the Maz shear zone of 427 Ma from both the Zaino (427 ± 4.5 Ma) and Maz (427.2 ± 6 Ma) Complexes constrains the timing of initial deformation, while matrix monazite ages date the timing of continued or later metamorphism and deformation between 418 Ma and 410 Ma.

The Ramaditas Complex exposed just east of the Sierra de Maz (Fig. 2) experienced Ordovician low- to medium-pressure and high-temperature granulite facies metamorphism and younger Silurian deformation and/or metamorphism (Fig. 11). Garnet and sillimanite ± cordierite-bearing metapelites record peak metamorphism at ~5.5 kbar and 775–850 °C (Fig. 7A) at 461 ± 11 Ma (garnet Lu-Hf) and 462 ± 4 Ma (monazite U-Pb). Monazite in the sillimanite-bearing matrix of metapelites dates younger deformation and metamorphism at 426 ± 11 Ma. Casquet et al. (2008b) reported U-Pb ages from zircon rims in the Sierra Ramaditas that similarly range from 465 Ma to 425 Ma that are consistent with these ages and, taken together, suggest either two distinct events or prolonged Ordovician to Silurian metamorphism and deformation.

The geochronology (Fig. 11) and metamorphic conditions of different litho-tectonic units within the Sierra de Maz suggest that the individual units experienced markedly different tectonic histories from one another and potentially from other metamorphic units within the Western Sierras Pampeanas (Fig. 12). The Taco Complex has been variably correlated with the Ramaditas Complex (e.g., Porcher et al., 2004; Varela et al., 2011), the Maz Complex (Kilmurray and Dalla Salda, 1971), or included with the Zaino Complex into the Western Domain (e.g., Casquet et al., 2006; Colombo et al., 2009; Rapela et al., 2010). The Taco and Ramaditas Complexes both record Ordovician (ca. 470–460 Ma) metamorphism (Fig. 11); however, the Taco Complex records lower a peak metamorphic temperature and higher pressure (~680 °C, ~6.5 kbar) than the Ramaditas Complex (≥800 °C, <5.5 kbar). The timing and conditions of metamorphism therefore support separating the Taco Complex as distinct from the Ramaditas Complex as well as other high-grade units in the Sierra de Maz (Fig. 2). Instead, the Taco Complex may be regionally correlative with units in the Central Complex of the Sierra de Pie de Palo and/or Sierra de Umango because they have similar protoliths, peak metamorphic conditions, and metamorphic ages (e.g., Mulcahy et al., 2011; Varela et al., 2011; Meira et al., 2012; Ramacciotti et al., 2019a) (Figs. 11–12). Instead, the Ramaditas Complex best correlates regionally with similar Ordovician (ca. 480–455 Ma) sillimanite and cordierite-bearing granulite facies units east of the Valle Fértil lineament and within the Famatina arc (Figs. 11–12) that are exposed in Sierras de Valle Fértil–La Huerta and in Villa Castelli (e.g., Casquet et al., 2006; Otamendi et al., 2008; Colombo et al., 2009; Rapela et al., 2010; Alasino et al., 2014).

The Zaino and Maz Complexes have distinctly unique metamorphic histories compared to other litho-tectonic units within the Sierra de Maz and the Western Sierra Pampeanas (Figs. 11–12). Thus far, both units lack evidence, in the form of garnet and monazite ages, of having experienced the Ordovician Famatinian orogeny (ca. 490–455 Ma) and instead record younger Paleozoic metamorphism ca. 430–410 Ma (Fig. 11). Metamorphic ages in the Zaino Complex do not support proposed correlations with the Difunta Correa metasedimentary sequence in the Sierra de Pie de Palo that experienced metamorphism and magmatism between 475 Ma and 460 Ma (e.g., Mulcahy et al., 2011; Ramacciotti et al., 2019a, 2019b). In addition, the Maz Complex records an earlier granulite facies event at ca. 1.2 Ga (Casquet et al., 2005, 2006; Rapela et al., 2010; this study) that is absent in other units of the Sierra Maz, such as the Taco, Ramaditas, and Zaino Complexes. Whether or not the Zaino Complex is distinct from the Maz Complex or, alternatively, is a younger cover sequence of the Maz Complex remains to be tested with detrital and provenance ages across the two units.

The timing of metamorphism and magmatism within the Zaino and Maz Complexes suggests these units may be correlative with the Resina Complex and distinct from other regional metamorphic terranes (Fig. 12). Ca. 1.2 Ga Proterozoic ages have been reported from other metamorphic regions of the Western Sierras Pampeanas (e.g., Kay et al., 1996; Varela et al., 2003; Sato et al., 2004; Vujovich et al., 2004), however, the presence of ca. 840 Ma orthogneiss ages appears to be unique to the Maz Complex (Colombo et al., 2009) and the Resina Complex (McClelland et al., 2005), a narrow, fault-bounded unit within the Valle Fértil fault zone between the Famatina arc and the Western Sierras Pampeanas (Fig. 12). If this proposed correlation is correct, the MARA terrane as defined within the Western Sierras Pampeanas (Fig. 1) is problematic because, even though some lithologies and protolith ages of units correlate along strike, the timing of Paleozoic metamorphism and deformation (Fig. 11) and the metamorphic conditions (Fig. 12) do not.

Evidence for a component of strike-slip deformation within middle- and lower-crustal rocks of the Western Sierras Pampeanas suggests a fundamental transition in the tectonic setting of the Gondwana margin. During the Ordovician (ca. 470–440 Ma), middle- and lower-crustal shear zones exposed in the Sierra de Pie de Palo dominantly record top-to-the-west oblique convergence that was synchronous with extensive arc magmatism (e.g., Mulcahy et al., 2011, 2014). In contrast, garnet ages (427 ± 4.5 Ma, 427.2 ± 6.3 Ma) and matrix monazite ages (418.7 ± 3.6 Ma) within the Maz shear zone overlap within uncertainty at ca. 422 Ma and are interpreted to record sinistral deformation within the Zaino and Maz Complexes at that time. Younger monazite ages (413 ± 7 Ma and 410 ± 4 Ma) in the Maz Complex may record some component of strike-slip deformation into the Devonian. The timing and kinematics of deformation on the Ramaditas shear zone are less constrained, but ca. 426 Ma matrix monazite and rims on older monazite suggest the shear zone was at least active at that time. Taken together, the data suggest the dominantly convergent Ordovician (470–440 Ma) margin transitioned to a highly oblique margin in the Silurian and Devonian (427–410 Ma).

The timing of metamorphism and deformation within the Sierra de Maz does not support a Cambrian collision of the MARA terrane with the

Gondawana margin (e.g., Casquet et al., 2012; Rapela et al., 2016). There is little evidence of Cambrian metamorphism or convergent deformation within the Zaino and Maz Complexes. In contrast, the timing of prograde to peak metamorphism in the Zaino Complex (ca. 427–419 Ma); younger metamorphic overprints (426–410 Ma) in the Taco, Maz, and Ramaditas Complexes; and the timing of strike-slip deformation on the Maz and Ramaditas shear zones (ca. 430–410 Ma) imply the region was affected by a significant tectonic event in the Silurian-Devonian. Evidence for strike-slip deformation within the Zaino and Maz Complexes in the Sierra de Maz and along strike within the Valle Fértil lineament farther south (e.g., McClelland et al., 2005; Mulcahy et al., 2014) suggest that at least some of the units interpreted as the MARA terrane were emplaced along the Gondwana margin by a component of translation.

REFERENCES CITED

Alasino, P.H., Casquet, C., Larrovere, M.A., Pankhurst, R.J., Galindo, C., Dahlquist, J.A., Baldo, E.G., and Rapela, C.W., 2014, The evolution of a mid-crustal thermal aureole at Cerro Toro, Sierra de Famatina, NW Argentina: Lithos, v. 190, p. 154–172, https://doi.org/10.1016/j.lithos.2013.12.006.

Bouvier, A., Vervoort, J.D., and Patchett, P.J., 2008, The Lu–Hf and Sm–Nd isotopic composition of CHUR: Constraints from unequilibrated chondrites and implications for the bulk composition of terrestrial planets: Earth and Planetary Science Letters, v. 273, p. 48–57, https://doi.org/10.1016/j.epsl.2008.06.010.

Büttner, S., Glodny, J., Lucassen, F., Wemmer, K., Erdmann, S., Handler, R., and Franz, G., 2005, Ordovician metamorphism and plutonism in the Sierra de Quilmes metamorphic complex: Implications for the tectonic setting of the northern Sierras Pampeanas (NW Argentina): Lithos, v. 83, p. 143–181, https://doi.org/10.1016/j.lithos.2005.01.006.

Casquet, C., Baldo, E., Pankhurst, R.J., Rapela, C.W., Galindo, C., Fanning, C.M., and Saavedra, J., 2001, Involvement of the Argentine Precordillera terrane in the Famatinian mobile belt: U-Pb SHRIMP and metamorphic evidence from the Sierra de Pie de Palo: Geology, v. 29, p. 703–706, https://doi.org/10.1130/0091-7613(2001)029<0703:IOTAPT>2.0.CO;2.

Casquet, C., Pankhurst, R.J., Rapela, C.W., Galindo, C., Dahlquist, J., Baldo, E., Saavedra, J., Casado, J.G., and Fanning, C.M., 2005, Grenvillian massif-type anorthosites in the Sierras Pampeanas: Journal of the Geological Society, v. 162, p. 9–12, https://doi.org/10.1144/0016-764904-100.

Casquet, C., Pankhurst, R.J., Fanning, C.M., Baldo, E., Galindo, C., Rapela, C.W., González-Casado, J.M., and Dahlquist, J.A., 2006, U–Pb SHRIMP zircon dating of Grenvillian metamorphism in Western Sierras Pampeanas (Argentina): Correlation with the Arequipa-Antofalla craton and constraints on the extent of the Precordillera Terrane: Gondwana Research, v. 9, p. 524–529, https://doi.org/10.1016/j.gr.2005.12.004.

Casquet, C., Pankhurst, R.J., Galindo, C., Rapela, C., Fanning, C.M., Baldo, E., Dahlquist, J., Casado, J.M.G., and Colombo, F., 2008a, A deformed alkaline igneous rock–carbonatite complex from the Western Sierras Pampeanas, Argentina: Evidence for late Neoproterozoic opening of the Clymene Ocean?: Precambrian Research, v. 165, p. 205–220, https://doi.org/10.1016/j.precamres.2008.06.011.

Casquet, C., Pankhurst, R.J., Rapela, C.W., Galindo, C., Fanning, C.M., Chiaradia, M., Baldo, E., González-Casado, J.M., and Dahlquist, J.A., 2008b, The Mesoproterozoic Maz terrane in the Western Sierras Pampeanas, Argentina, equivalent to the Arequipa–Antofalla block of southern Peru? Implications for West Gondwana margin evolution: Gondwana Research, v. 13, p. 163–175, https://doi.org/10.1016/j.gr.2007.04.005.

Casquet, C., Rapela, C.W., Pankhurst, R.J., Baldo, E.G., Galindo, C., Fanning, C.M., Dahlquist, J.A., and Saavedra, J., 2012, A history of Proterozoic terranes in southern South America: From Rodinia to Gondwana: Geoscience Frontiers, v. 3, p. 137–145, https://doi.org/10.1016/j.gsf.2011.11.004.

Colombo, F., Baldo, E.G.A., Casquet, C., Pankhurst, R.J., Galindo, C., Rapela, C.W., Dahlquist, J.A., and Fanning, C.M., 2009, A-type magmatism in the sierras of Maz and Espinal: A new record of Rodinia break-up in the Western Sierras Pampeanas of Argentina: Precambrian Research, v. 175, p. 77–86, https://doi.org/10.1016/j.precamres.2009.08.006.

Dale, J., Holland, T., and Powell, R., 2000, Hornblende–garnet–plagioclase thermobarometry: A natural assemblage calibration of the thermodynamics of hornblende: Contributions to Mineralogy and Petrology, v. 140, p. 353–362, https://doi.org/10.1007/s004100000187.

de Capitani, C., and Petrakakis, K., 2010, The computation of equilibrium assemblage diagrams with Theriak/Domino software: The American Mineralogist, v. 95, p. 1006–1016, https://doi.org/10.2138/am.2010.3354.

Ferry, J.M., and Spear, F.S., 1978, Experimental calibration of the partitioning of Fe and Mg between biotite and garnet: Contributions to Mineralogy and Petrology, v. 66, p. 113–117, https://doi.org/10.1007/BF00372150.

Finch, M.A., Weinberg, R.F., Hasalová, P., Becchio, R., Fuentes, M.G., and Kennedy, A., 2017, Tectono-metamorphic evolution of a convergent back-arc: The Famatinian orogen, Sierra de Quilmes, Sierras Pampeanas, NW Argentina: Geological Society of America Bulletin, v. 129, p. 1602–1621, https://doi.org/10.1130/B31620.1.

Florence, F.P., and Spear, F.S., 1995, Intergranular diffusion kinetics of Fe and Mg during retrograde metamorphism of a pelitic gneiss from the Adirondack Mountains: Earth and Planetary Science Letters, v. 134, p. 329–340, https://doi.org/10.1016/0012-821X(95)00129-Z.

Galindo, C., Murra, J., Baldo, E., Casquet, C., Rapela, C., Pankhurst, R., and Dahlquist, J., 2004, Datación Sm-Nd del metamorfismo en la Sierra de la Imanas (Sierras Pampeanas Occidentales, Argentina): Geogaceta, v. 35, p. 75–78.

Gallien, F., Mogessie, A., Bjerg, E., Delpino, S., de Machuca, B.C., Thöni, M., and Klötzli, U., 2010, Timing and rate of granulite facies metamorphism and cooling from multi-mineral chronology on migmatitic gneisses, Sierras de La Huerta and Valle Fértil, NW Argentina: Lithos, v. 114, p. 229–252, https://doi.org/10.1016/j.lithos.2009.08.011.

Garber, J.M., Roeske, S.M., Warren, J., Mulcahy, S.R., McClelland, W.C., Austin, L.J., Renne, P.R., and Vujovich, G.I., 2014, Crustal shortening, exhumation, and strain localization in a collisional orogen: The Bajo Pequeño Shear Zone, Sierra de Pie de Palo, Argentina: Tectonics, v. 33, https://doi.org/10.1002/2013TC003477.

Graham, C.M., and Powell, R., 1984, A garnet–hornblende geothermometer: Calibration, testing, and application to the Pelona Schist, Southern California: Journal of Metamorphic Geology, v. 2, p. 13–31, https://doi.org/10.1111/j.1525-1314.1984.tb00282.x.

Grissom, G.C., Debari, S.M., and Snee, L.W., 1998, Geology of the Sierra de Fiambalá, northwestern Argentina: Implications for early Palaeozoic Andean tectonics, in Pankhurst, R.J., and Rapela, C.W., eds., The Proto-Andean Margin of Gondwana: Geological Society, London, Special Publication 142, p. 297–323, https://doi.org/10.1144/GSL.SP.1998.142.01.15.

Hodges, K., and Spear, F.S., 1982, Geothermometry, geobarometry and the Al_2SiO_5 triple point at Mt. Moosilauke, New Hampshire: The American Mineralogist, v. 67, p. 1118–1134.

Hoisch, T.D., 1990, Empirical calibration of six geobarometers for the mineral assemblage quartz+muscovite+biotite+plagioclase+garnet: Contributions to Mineralogy and Petrology, v. 104, p. 225–234, https://doi.org/10.1007/BF00306445.

Holland, T., and Powell, R., 1992, Plagioclase feldspars: Activity-composition relations based upon Darken's quadratic formalism and Landau theory: The American Mineralogist, v. 77, p. 53–61.

Holland, T., and Powell, R., 1998, An internally consistent thermodynamic data set for phases of petrological interest: Journal of Metamorphic Geology, v. 16, p. 309–343, https://doi.org/10.1111/j.1525-1314.1998.00140.x.

Holland, T., Baker, J., and Powell, R., 1998, Mixing properties and activity-composition relationships of chlorites in the system MgO-FeO-Al_2O_3-SiO_2-H_2O: European Journal of Mineralogy, v. 10, p. 395–406, https://doi.org/10.1127/ejm/10/3/0395.

Kay, S.M., Orrell, S., and Abbruzzi, J.M., 1996, Zircon and whole rock Nd-Pb isotopic evidence for a Grenville age and a Laurentian origin for the basement of the Precordillera in Argentina: The Journal of Geology, v. 104, p. 637–648, https://doi.org/10.1086/629859.

Kilmurray, J.O., and Dalla Salda, L., 1971, Las fases de deformación y metamorfismo en la Sierra de Maz, provincia de La Rioja, República Argentina: Revista de la Asociación Geológica Argentina, v. 26, p. 245–263.

Kohn, M.J., 2009, Models of garnet differential geochronology: Geochimica et Cosmochimica Acta, v. 73, p. 170–182, https://doi.org/10.1016/j.gca.2008.10.004.

Koziol, A.M., and Newton, R.C., 1988, Redetermination of the anorthite breakdown reaction and improvement of the plagioclase-garnet-Al₂SiO₅-quartz geobarometer: The American Mineralogist, v. 73, p. 216–223.

Lucassen, F., and Becchio, R., 2003, Timing of high-grade metamorphism: Early Palaeozoic U–Pb formation ages of titanite indicate long-standing high-T conditions at the western margin of Gondwana (Argentina, 26–29°S): Journal of Metamorphic Geology, v. 21, p. 649–662, https://doi.org/10.1046/j.1525-1314.2003.00471.x.

Lucassen, F., Becchio, R., and Franz, G., 2010, The early Palaeozoic high-grade metamorphism at the active continental margin of West Gondwana in the Andes (NW Argentina/N Chile): International Journal of Earth Sciences, v. 100, p. 445–463, https://doi.org/10.1007/s00531-010-0585-3.

McClelland, W.C., Ellis, J.R., Roeske, S.M., Mulcahy, S.R., Vujovich, G.I., and Naipauer, M., 2005, U-Pb SHRIMP igneous zircon ages and LA-ICPMS detrital zircon ages from metamorphic rocks between the Precordillera terrane and the Gondwana margin, Sierra de la Huerta to Pie de Palo, northwest Argentina: Gondwana, v. 12, p. 250.

Meira, V.T., Campos Neto, M. da C., González, P.D., Stipp Basei, M.Â., and Varela, R., 2012, Ordovician klippen structures of the Sierra de Umango: New insights on tectonic evolution of the Western Sierras Pampeanas, Argentina: Journal of South American Earth Sciences, v. 37, p. 154–174, https://doi.org/10.1016/j.jsames.2012.02.002.

Mulcahy, S.R., Roeske, S.M., McClelland, W.C., Nomade, S., and Renne, P.R., 2007, Cambrian initiation of the Las Pirquitas thrust of the western Sierras Pampeanas, Argentina: Implications for the tectonic evolution of the proto-Andean margin of South America: Geology, v. 35, p. 443–446, https://doi.org/10.1130/G23436A.1.

Mulcahy, S.R., Roeske, S.M., McClelland, W.C., Jourdan, F., Iriondo, A., Renne, P.R., Vervoort, J.D., and Vujovich, G.I., 2011, Structural evolution of a composite middle to lower crustal section: The Sierra de Pie de Palo, northwest Argentina: Tectonics, v. 30, no. 1, https://doi.org/10.1029/2009TC002656.

Mulcahy, S.R., Roeske, S.M., McClelland, W.C., Ellis, J.R., Jourdan, F., Renne, P.R., Vervoort, J.D., and Vujovich, G.I., 2014, Multiple migmatite events and cooling from granulite facies metamorphism within the Famatina arc margin of northwest Argentina: Tectonics, v. 33, p. 1–25, https://doi.org/10.1002/2013TC003398.

Otamendi, J.E., Tibaldi, A.M., Vujovich, G.I., and Viñao, G.A., 2008, Metamorphic evolution of migmatites from the deep Famatinian arc crust exposed in Sierras Valle Fértil–La Huerta, San Juan, Argentina: Journal of South American Earth Sciences, v. 25, p. 313–335, https://doi.org/10.1016/j.jsames.2007.09.001.

Perchuk, L., Aranovich, L.Y., Podlesskii, K., Lavrant'eva, I., Gerasimov, V.Y., Fed'Kin, V., Kitsul, V., Karsakov, L., and Berdnikov, N., 1985, Precambrian granulites of the Aldan shield, eastern Siberia, USSR: Journal of Metamorphic Geology, v. 3, p. 265–310, https://doi.org/10.1111/j.1525-1314.1985.tb00321.x.

Porcher, C.C., Fernandes, L.A., Vujovich, G.I., and Chernicoff, C.J., 2004, Thermobarometry, Sm/Nd ages and geophysical evidence for the location of the suture zone between Cuyania and the western proto-Andean margin of Gondwana: Gondwana Research, v. 7, p. 1057–1076, https://doi.org/10.1016/S1342-937X(05)71084-4.

Powell, R., and Holland, T., 1994, Optimal geothermometry and geobarometry: The American Mineralogist, v. 79, p. 120–133, http://www.minsocam.org/ammin/AM79/AM79_120.pdf (accessed April 2021).

Powell, R., and Holland, T., 1999, Relating formulations of the thermodynamics of mineral solid solutions: Activity modeling of pyroxenes, amphiboles, and micas: The American Mineralogist, v. 84, p. 1–14, https://doi.org/10.2138/am-1999-1-201.

Powell, R., and Holland, T., 2010, Using equilibrium thermodynamics to understand metamorphism and metamorphic rocks: Elements, v. 6, p. 309–314, https://doi.org/10.2113/gselements.6.5.309.

Ramacciotti, C.D., Casquet, C., Baldo, E.G., Alasino, P.H., Galindo, C., and Dahlquist, J.A., 2019a, Late Cambrian–Early Ordovician magmatism in the Sierra de Pie de Palo, Sierras Pampeanas (Argentina): Implications for the early evolution of the proto-Andean margin of Gondwana: Geological Magazine, v. 157, p. 1–19, https://doi.org/10.1017/S0016756819000748.

Ramacciotti, C.D., Casquet, C., Baldo, E.G., Verdecchia, S.O., Morales Cámera, M.M., and Zandomeni, P.S., 2019b, Metamorfismo de alto gradiente P/T en la Sierra de Pie de Palo (Sierras Pampeanas, Argentina): Modelado de equilibrio de fases minerales e implicancias geodinámicas en el antearco famatiniano: Andean Geology, v. 46, p. 526–555, https://doi.org/10.5027/andgeoV46n3-3198.

Ramos, V.A., 2018, The Famatinian Orogen along the protomargin of Western Gondwana: Evidence for a nearly continuous Ordovician magmatic arc between Venezuela and Argentina, in Folguera, A., et al., eds., The Evolution of the Chilean-Argentinean Andes: Cham, Switzerland, Springer International Publishing, Springer Earth System Sciences, p. 133–161, https://doi.org/10.1007/978-3-319-67774-3_6.

Ramos, V.A., Dallmeyer, R.D., and Vujovich, G., 1998, Time constraints on the early Palaeozoic docking of the Precordillera, central Argentina, in Pankhurst, R.J., and Rapela, C.W., eds., The Proto-Andean Margin of Gondwana: Geological Society, London, Special Publication 142, p. 143–158, https://doi.org/10.1144/GSL.SP.1998.142.01.08.

Rapela, C.W., Pankhurst, R., Casquet, C., Fanning, C., Galindo Francisco, M., and Baldo, E.G., 2005, Datación U-Pb SHRIMP de circones detríticos en paranfibolitas neoproterozoicas de las secuencia Difunta Correa (Sierras Pampeanas Occidentales): Geogaceta, v. 38, p. 227–230, https://sge.usal.es/archivos/geogacetas/Geo38/Geo38-57.pdf (accessed April 2021).

Rapela, C.W., Pankhurst, R.J., Casquet, C., Baldo, E., Galindo, C., Fanning, C.M., and Dahlquist, J.M., 2010, The Western Sierras Pampeanas: Protracted Grenville-age history (1330–1030 Ma) of intra-oceanic arcs, subduction–accretion at continental-edge and AMCG intraplate magmatism: Journal of South American Earth Sciences, v. 29, p. 105–127, https://doi.org/10.1016/j.jsames.2009.08.004.

Rapela, C.W., Verdecchia, S.O., Casquet, C., Pankhurst, R.J., Baldo, E.G., Galindo, C., Murra, J.A., Dahlquist, J.A., and Fanning, C.M., 2016, Identifying Laurentian and SW Gondwana sources in the Neoproterozoic to Early Paleozoic metasedimentary rocks of the Sierras Pampeanas: Paleogeographic and tectonic implications: Gondwana Research, v. 32, p. 193–212, https://doi.org/10.1016/j.gr.2015.02.010.

Rapela, C.W., Pankhurst, R.J., Casquet, C., Dahlquist, J.A., Fanning, C.M., Baldo, E.G., Galindo, C., Alasino, P.H., Ramacciotti, C.D., and Verdecchia, S.O., 2018, A review of the Famatinian Ordovician magmatism in southern South America: Evidence of lithosphere reworking and continental subduction in the early proto-Andean margin of Gondwana: Earth-Science Reviews, v. 187, p. 259–285, https://doi.org/10.1016/j.earscirev.2018.10.006.

Sato, A.M., Tickyj, H., Llambías, E.J., Stipp Basei, M.A., and González, P.D., 2004, Las Matras Block, Central Argentina (37°S-67°W): The southernmost Cuyania terrane and its relationship with the Famatinian Orogeny: Gondwana Research, v. 7, p. 1077–1087, https://doi.org/10.1016/S1342-937X(05)71085-6.

Scherer, E., Münker, C., and Mezger, K., 2001, Calibration of the lutetium-hafnium clock: Science, v. 293, p. 683–687, https://doi.org/10.1126/science.1061372.

Söderlund, U., Patchett, P.J., Vervoort, J.D., and Isachsen, C.E., 2004, The ¹⁷⁶Lu decay constant determined by Lu–Hf and U–Pb isotope systematics of Precambrian mafic intrusions: Earth and Planetary Science Letters, v. 219, p. 311–324, https://doi.org/10.1016/S0012-821X(04)00012-3.

Spear, F.S., and Cheney, J.T., 1989, A petrogenetic grid for pelitic schists in the system SiO₂-Al₂O₃-FeO-MgO-K₂O–H₂O: Contributions to Mineralogy and Petrology, v. 101, p. 149–164, https://doi.org/10.1007/BF00375302.

Spear, F.S., Kohn, M.J., and Cheney, J.T., 1999, P-T paths from anatectic pelites: Contributions to Mineralogy and Petrology, v. 134, p. 17–32, https://doi.org/10.1007/s004100050466.

Steenken, A., Siegesmund, S., de Luchi, M.G.L., Frei, R., and Wemmer, K., 2006, Neoproterozoic to Early Palaeozoic events in the Sierra de San Luis: Implications for the Famatinian geodynamics in the Eastern Sierras Pampeanas (Argentina): Journal of the Geological Society, v. 163, p. 965–982, https://doi.org/10.1144/0016-76492005-064.

Tibaldi, A.M., Otamendi, J.E., Cristofolini, E.A., Baliani, I., Walker, B.A., Jr., and Bergantz, G.W., 2013, Reconstruction of the early Ordovician Famatinian arc through thermobarometry in lower and middle crustal exposures, Sierra de Valle Fértil, Argentina: Tectonophysics, v. 589, p. 151–166, https://doi.org/10.1016/j.tecto.2012.12.032.

Tuccillo, M.E., Essene, E.J., and van der Pluijm, B.A., 1990, Growth and retrograde zoning in garnets from high-grade, metapelites: Implications for pressure-temperature paths: Geology, v. 18, p. 839–842, https://doi.org/10.1130/0091-7613(1990)018<0839:GARZIG>2.3.CO;2.

Varela, R., Basei, M.A.S., Sato, A.M., González, P.D., Siga, O., Jr., Campos Neto, M., and da Costa, C.C., 2003, Grenvillian basement and Famatinian events of the Sierra de Umango (29°S): A review and new geochronological data, in Proceedings of the IV South American Symposium on Isotope Geology, v. 1, p. 304–306.

Varela, R., Basei, M.A.S., González, P.D., Sato, A.M., Naipauer, M., Campos Neto, M., Cingolani, C.A., and Meira, V.T., 2011, Accretion of Grenvillian terranes to the southwestern border of

the Río de la Plata craton, western Argentina: International Journal of Earth Sciences, v. 100, p. 243–272, https://doi.org/10.1007/s00531-010-0614-2.

Vermeesch, P., 2018, IsoplotR: A free and open toolbox for geochronology: Geoscience Frontiers, v. 9, p. 1479–1493, https://doi.org/10.1016/j.gsf.2018.04.001.

Vujovich, G.I., and Kay, S.M., 1998, A Laurentian? Grenville-age oceanic arc/back-arc terrane in the Sierra de Pie de Palo, Western Sierras Pampeanas, Argentina, *in* Pankhurst, R.J., and Rapela, C.W., eds., The Proto-Andean Margin of Gondwana: Geological Society, London, Special Publication 142, p. 159–179, https://doi.org/10.1144/GSL.SP.1998.142.01.09.

Vujovich, G.I., van Staal, C.R., and Davis, W., 2004, Age constraints on the tectonic evolution and provenance of the Pie de Palo Complex, Cuyania composite terrane, and the Famatinian orogeny in the Sierra de Pie de Palo, San Juan, Argentina: Gondwana Research, v. 7, p. 1041–1056, https://doi.org/10.1016/S1342-937X(05)71083-2.

Whitney, D.L., and Evans, B.W., 2010, Abbreviations for names of rock-forming minerals: The American Mineralogist, v. 95, p. 185–187, https://doi.org/10.2138/am.2010.3371.

Wu, C., 2015, Revised empirical garnet–biotite–muscovite–plagioclase geobarometer in metapelites: Journal of Metamorphic Geology, v. 33, p. 167–176, https://doi.org/10.1111/jmg.12115.